Variational formulation for helical cracks

Kaushik Vijaykumar[a], David Henann[a], Haneesh Kesari[a,*]

[a]*Engineering, Brown University, Providence, RI-02906*

Abstract

Text of abstract.

Keywords: Variational formulation, helical symmetry, curvilinear coordinates, curvilinear FEA

1. Introduction

A material when subjected to tensile stresses far exceeding its bond strength, tends to form cracks to relieve the high stresses. Cracks or crack patterns can be of various types such as, cleavage cracks [1], mud cracks [2, 3], wavy cracks [4, 5, 6, 7], spiral cracks [8, 9, 10] to name a few. It is postulated that the occurrence of the type of crack pattern is governed by the amount of strain energy that the material can release [11, 12]. In other words, crack pattern that releases the maximum strain energy for the given loading state is the one that will occur. For instance, a typical failure mechanism in brittle materials such as, glass, when under tensile loads is cleavage however, these materials are also observed to form spiral cracks as seen in Fig. 1(a). The modes of fracture such as spirals dissipate more energy as compared to a cleavage crack and present an effective way of converting strain energy to surface energy. Therefore, in certain loading conditions they are energetically favorable as compared to cleavage cracking or fragmentation.

John hopfield [11] proposed a methodology to create spiral cracks by conducting experiments on hollow Pyrex glass tubes. One end of the glass tube is brought into contact with a hot plate at 500-600°C and held briefly before suddenly cooling it in cold water. The sudden quenching of the glass tube leads to state of tensile stress on the outer surface of the glass while the inner surface is under compressive stress. Contrary to the expectation that glass being a brittle material will shatter to relieve the tensile stress on the outer surface, it forms a spiral pattern to relieve the tensile stress (see Fig. 1(a)). It is believed that formation of spiral cracks is an efficient mechanism to release the excess strain energy as compared to fragmentation. Gillham et al. [12] proposed a systematic set of experiments to produce helical and spiral fractures. It was shown that helical and spiral fractures could be produced in a brittle glass yarn cured in a polymeric resin by quenching it after cure. One such image of the formation of a helical fracture pattern is shown in Fig. 1(b). Such patterns have also

*Corresponding author

Email address: haneesh_kesari@brown.edu (Haneesh Kesari)

been observed in *Monorhaphis chuni* (*M.chuni*), which is a biological composite material. The microstructure of *M.chuni* resembles that of a lamellar structure, where a brittle mineral phase is arranged concentrically and is separated by a nanometer-thin layer ($\approx 35nm$ [13]) of a soft organic phase. Fracture morphology of *Monorhaphis chuni* samples subjected to three point bending test reveal failure by crack deflection. However, in some samples of *M.chuni*, instead of crack deflection at the organic interlayers, helical fracture is seen as a preferred failure mode. The helical fracture pattern observed in *Monorhaphis chuni* sample, reported by [14], is shown in Fig. 1(c).

Predicting and quantifying the nature of such complex crack patterns is a challenge. Freund and Kim [15], studied failure in brittle substrates due to residual stresses produced by cooling of molten metal in the substrate cavities. They predicted the formation of spiral fracture emanating from the substrate-metal interface using the crack growth criterion $K_{II} = 0$. Xia and Hutchinson [16], studied the formation of spiral patterns in thin films bonded to substrates to gain insights into the experimental observations of spiral cracks in thin films (see [17, 18]). They adopted the distributed dislocation approach to model the spiral cracks and found that spiral cracks form only in the presence of spiral shaped flaws.

2. Linear thermo-elasticity in helical coordinates

As mentioned in the introduction, we are studying the occurrence of helical cracks in thermally heated cylinders. The main objective of this work is to be able to predict the pitch of the helix that will occur given a temperature distribution (i.e., $\Delta T(\rho, \zeta)$) and surface energy. A continuum mechanics based linear thermo-elasticity theory is formulated terms of helical coordinates. The advantages of such a formulation is as follows:

1. A 3D elasticity problem would involve development of series of meshes of a cylinder with a helical crack for different pitches. The problem needs to be solved for a given temperature distribution to obtain the strain energy for different pitches. However, mesh development is a cumbersome process and prescribing boundary conditions is not straight forward.
2. On choosing the temperature to depend on (ρ, ζ), the boundary value problem is symmetric along the pitch of the helix. A boundary value problem is helically symmetric if none of the fields change for a fixed (ρ, ζ), for any change in ϕ. Imposing helical symmetry can simplify the problem for 3D to 2D problem in just (ρ, ζ) analogous to the axis-symmetric problems in cylindrical coordinates. However, if 3D elasticity is employed then imposing this symmetry is not possible.

2.1. General linear thermo-elastic constitutive equations

In this section, a continuum mechanics based linear thermo-elastic theory will be detailed. Some of the important concepts of continuum mechanics theory in the following sections is reviewed from Gurtin [19] and Jog [20]. A brief review of curvilinear coordinates is also provided from Green and Zerna [21] in order to facilitate the derivation of the linear thermo-elastic theory in helical coordinates.

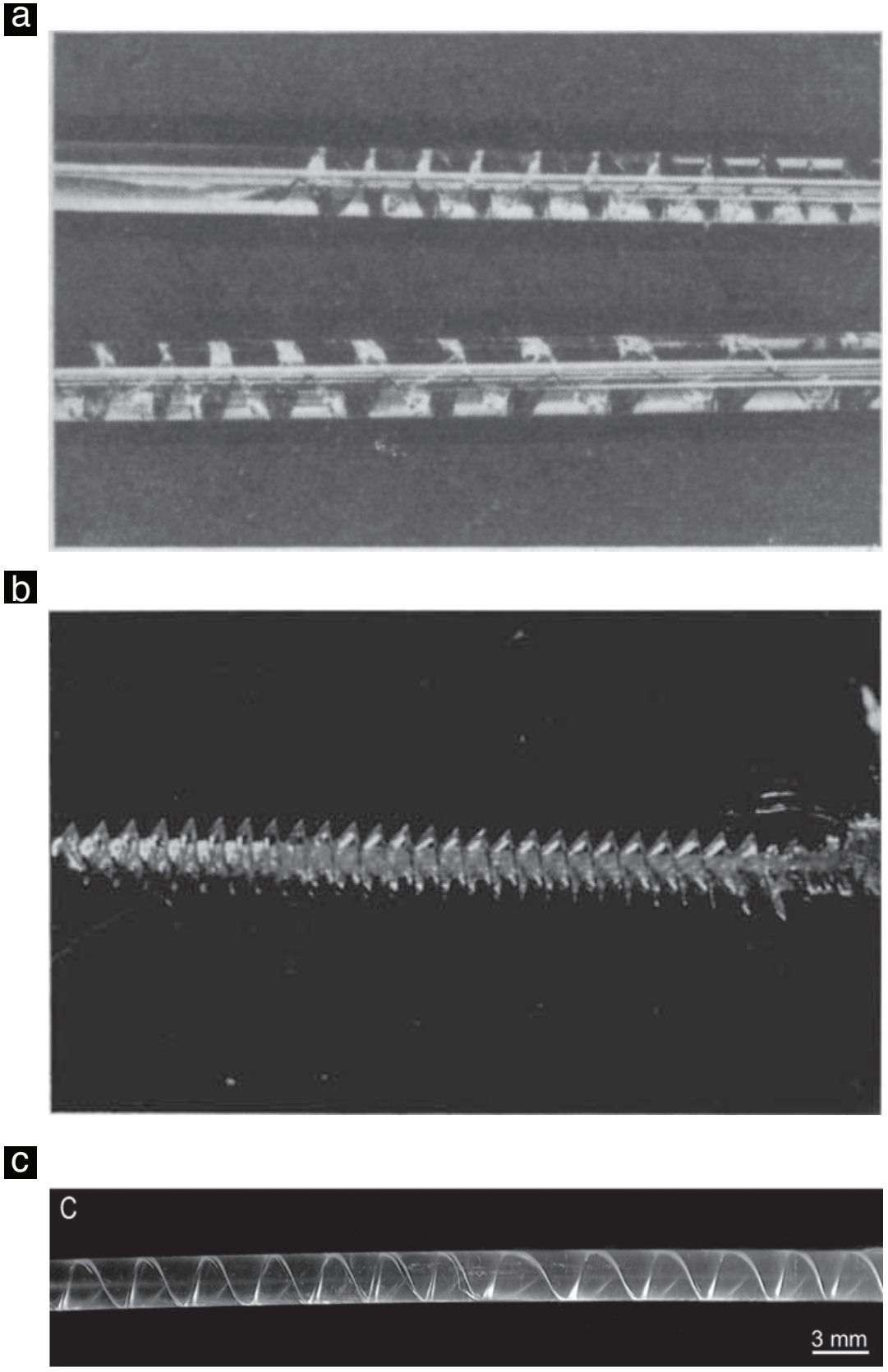

{intro}

Figure 1: In this figure, spiral and helical crack patterns are shown. In subfigure(a)

2.1.1. Mathematical preliminaries

Some of the fundamental concepts of continuum mechanics are briefly reviewed here from Gurtin [19] and Jog [20]. The following sets will be referred to in the formulation of linear thermo-elastic continuum mechanics theory.

- Lin = the set of all tensors;
- Lin^+ = the set of all tensors $\mathbf{S}$ with $\det \mathbf{S} > 0$;
- Sym = the set of all symmetric tensors;
- Skw = the set of all skew-symmetric tensors;
- Psym = the set of all symmetric, positive definite tensors;
- $\mathbb{R}$ is the space of reals;
- $\mathbb{R}^+$ is the space of positive reals.

Let $\mathscr{E}$ be a three dimensional euclidean point space and $\mathscr{V}$ be a vector space such that $\mathscr{V} \subset \mathscr{E}$. The inner product of two vectors $\mathbf{u}$ and $\mathbf{v}$ is denoted as $\mathbf{u} \cdot \mathbf{v}$ for $\mathbf{u}, \mathbf{v} \in \mathscr{V}$. The magnitude of $\mathbf{v}$ denoted by $|\mathbf{v}| : \mathscr{V} \to \mathbb{R}^+$ is defined as,

agnitude}
$$|\mathbf{v}| = (\mathbf{v} \cdot \mathbf{v})^{1/2} . \tag{1}$$

A second order tensor $\mathbf{S} : \mathscr{V} \to \mathscr{V}$, such that

$$\mathbf{u} = \mathbf{S}\mathbf{v},$$

for all $\mathbf{u}, \mathbf{v} \in \mathscr{V}$. The identity tensor $\mathbf{I} : \mathscr{V} \to \mathscr{V}$ is defined as,

$$\mathbf{I}\,\mathbf{v} = \mathbf{v},$$

for all $\mathbf{v} \in \mathscr{V}$. The transpose of tensor $\mathbf{S}$ denoted by $\mathbf{S}^{\mathrm{T}}$ and can be defined as a unique tensor which satisfies

$$\mathbf{S}\mathbf{u} \cdot \mathbf{v} = \mathbf{u} \cdot \mathbf{S}^{\mathrm{T}}\mathbf{v},$$

for all $\mathbf{u}, \mathbf{v} \in \mathscr{V}$ and $\mathbf{S} \in \text{Lin}$. Further, the transpose operator $(\cdot)^{\mathrm{T}} : \text{Lin} \to \text{Lin}$. The tensor $\mathbf{S}$ is symmetric, i.e., $\mathbf{S} \in \text{Sym}$, if

$$\mathbf{S} = \mathbf{S}^{\mathrm{T}},$$

and the tensor $\mathbf{S} \in \text{Skw}$, if

$$\mathbf{S} = -\mathbf{S}^{\mathrm{T}}.$$

The determinant of tensor $\mathbf{S}$ is an operator denoted by $\det(\cdot) : \mathrm{Lin} \to \mathbb{R}$ and is given as,

$$\det \mathbf{S} = \det[\mathbf{S}],$$

where, $[\cdot]$ is the symbol for a matrix. The tensor product of two vectors $\mathbf{u}, \mathbf{v} \in \mathscr{V}$ denoted by $(\mathbf{u} \otimes \mathbf{v})$ is second order tensor. Therefore, for all $\mathbf{a} \in \mathscr{V}$, $(\mathbf{u} \otimes \mathbf{v}) : \mathscr{V} \to \mathscr{V}$ such that,

$$(\mathbf{u} \otimes \mathbf{v})\,\mathbf{a} = (\mathbf{v} \cdot \mathbf{a})\,\mathbf{u}.$$

Trace of tensor $\mathbf{S}$ denoted by $\mathrm{tr}\,\mathbf{S}$ is a linear operation such that $\mathrm{tr}(\cdot) : \mathrm{Lin} \to \mathbb{R}$ and satisfies,

$$\mathrm{tr}\,\mathbf{S} = \mathrm{tr}\,(\mathbf{u} \otimes \mathbf{v}) = \mathbf{u} \cdot \mathbf{v},$$

for all $\mathbf{u}, \mathbf{v} \in \mathscr{V}$ and $\mathbf{S} \in \mathrm{Lin}$. A tensor $\mathbf{S} \in \mathrm{Psym}$, if $\mathbf{S} \in \mathrm{Sym}$ and it satisfies,

$$\mathbf{v} \cdot \mathbf{S}\mathbf{v} > 0,$$

for $\mathbf{v} \neq \mathbf{0}$. The symbol $\mathbf{0}$ is a zero vector that maps every vector to a zero vector. The shorthand notation for a vector or a tensor using components will be employed in the rest of the work. A vector $\mathbf{u} \in \mathscr{V}$ in cartesian basis vectors, $\mathbf{e}_1 = (1,0,0)$, $\mathbf{e}_2 = (0,1,0)$ and $\mathbf{e}_3 = (0,0,1)$ can be expressed as

$$\mathbf{u} = \sum_{i=1}^{3} u_i\,\mathbf{e}_i,$$

and a second order tensor $\mathbf{S} \in \mathrm{Lin}$ is expressed as,

$$\mathbf{S} = \sum_{i,j=1}^{3} S_{ij}\,\mathbf{e}_i \otimes \mathbf{e}_j.$$

The symbols u_i and S_{ij} are the components of a vector and tensor, respectively. We can also define the summation rules as follows, let $\mathbf{v} = \mathbf{S}\mathbf{u}$, then the components v_i are given as,

$$v_i = \sum_{j=1}^{3} S_{ij}\,u_j,$$

where i is the free index and j is the dummy index which is summed because it is repeated twice. For brevity in the rest of the work, we will avoid the summation symbol.

To introduce differentiation of scalars, vectors and tensors, it is assumed that these mathematical quantities belong normed vector spaces wherever necessary (see [19]). Let $\mathscr{U} \subset \mathscr{E}$ and $\mathscr{W} \subset \mathscr{E}$ be finite dimensional normed vector spaces, such that $\mathscr{D} \subset \mathscr{U}$. Let $\mathbf{g} : \mathscr{D} \to \mathscr{W}$ be any tensor valued function. If there exists a derivative of $\mathbf{g}$ at $\mathbf{x} \in \mathscr{D}$ then there exists a linear transformation $D\mathbf{g}(\mathbf{x}) : \mathscr{U} \to \mathscr{W}$ which satisfies,

$$\mathbf{g}(\mathbf{x} + \mathbf{u}) = \mathbf{g}(\mathbf{x}) + D\mathbf{g}(\mathbf{x})[\mathbf{u}] + o(\mathbf{u}),$$

as $\mathbf{u} \to 0$ for all $\mathbf{u} \in \mathscr{D}$ and the operator $D\mathbf{g}(\mathbf{x})$ is called the derivative of $\mathbf{g}$ at $\mathbf{x}$. Further, the symbol o is called the little-o notation (see [19] for details). Therefore, we can define the gradient of a scalar field $\phi \in \mathscr{R} \subset \mathscr{E}$ and for each $\mathbf{x} \in \mathscr{R}$ as follows,

$$D\phi(\mathbf{x})[\mathbf{u}] = \boldsymbol{\nabla}\phi(\mathbf{x}) \cdot \mathbf{u},$$

where, $\boldsymbol{\nabla}$ is the gradient symbol and $\boldsymbol{\nabla}\phi(\mathbf{x}) : \mathbb{R} \to \mathscr{V}$ is the gradient of ϕ at $\mathbf{x}$. Similarly, the gradient of vector $\mathbf{v} \in \mathscr{V}$ is,

$$D\mathbf{v}(\mathbf{x})\,\mathbf{u} = \boldsymbol{\nabla}\mathbf{v}(\mathbf{x})[\mathbf{u}],$$

where $\boldsymbol{\nabla}\mathbf{v}(\mathbf{x}) : \mathscr{V} \to \mathscr{V}$ is the gradient of $\mathbf{v}$ at $\mathbf{x}$. We can also define divergence of a vector field $\mathbf{v}$ which is a scalar,

$$\operatorname{div} \mathbf{v} = \operatorname{tr} \boldsymbol{\nabla}\mathbf{v},$$

The divergence of a second order tensor $\mathbf{S}$ is an operation that satisfies,

$$(\operatorname{div} \mathbf{S}) \cdot \mathbf{a} = \operatorname{div} \left(\mathbf{S}^{\mathrm{T}}\mathbf{a}\right).$$

2.1.2. Kinematics

Let $\mathscr{B}$ be a bounded domain in $\mathscr{E}$ and can be referred to as the reference configuration. For each point $\mathbf{p} \in \mathscr{B}$ has an associated vector $\mathbf{R}$, denoted as the position vector of the point $\mathbf{p}$, such that $\mathbf{0} + \mathbf{R} = \mathbf{p}$. The symbol $\mathbf{0}$ is the origin and the point $\mathbf{p}$ is commonly called as the material point. To understand the deformation of the reference configuration $\mathscr{B}$ mathematically, a deformation mapping $\mathbf{f} : \mathscr{B} \to \mathscr{E}$ maps the material point $\mathbf{p}$ to a spatial point in a deformed configuration. Further, let $\mathbf{r}$ be the position vector of this spatial point from $\mathbf{0}$. The deformation mapping maps the quantities $\mathbf{R}$ and $\mathbf{r}$ referred as material and spatial position vectors, respectively, as follows,

$$\mathbf{r} = \mathbf{f}(\mathbf{R}).$$

To prevent interpenetration of the body $\mathscr{B}$ onto itself the mapping $\mathbf{f}$ is a one-to-one mapping and the mapping should be invertible. The restrictions on $\mathbf{f}$ will be discussed later on. The displacement field $\mathbf{u}$ is given as,

{disp}
$$\mathbf{u} = \mathbf{r} - \mathbf{R} = \mathbf{f}(\mathbf{R}) - \mathbf{R}. \tag{2}$$

The second order tensor $\mathbf{F} \in \mathrm{Lin}^{+}$, referred to as the deformation gradient, is given as,

tion_grad}
$$\mathbf{F}(\mathbf{R}) = \boldsymbol{\nabla}\mathbf{f}(\mathbf{R}), \tag{3}$$

where $\boldsymbol{\nabla}$ is the symbol for gradient in material coordinates. The quantity $\det \mathbf{F}$ represents the deformed volume element and has to satisfy $\det \mathbf{F} > 0$, so that a reference volume element is not mapped to a zero volume element. This condition imposes a restriction on $\mathbf{f}$, i.e.,

$\det \boldsymbol{\nabla}\mathbf{f} > 0$. The deformation gradient can also be expressed in terms of displacement using eqns. (2) and (3) as,

$$\mathbf{F} = \mathbf{I} + \boldsymbol{\nabla}\mathbf{u}.$$

The left and right Cauchy-Green strain tensors, $\mathbf{C}$ and $\mathbf{B}$ are,

$$\mathbf{C} = \mathbf{F}^{\mathsf{T}}\mathbf{F} = \mathbf{I} + \boldsymbol{\nabla}\mathbf{u} + \boldsymbol{\nabla}\mathbf{u}^{\mathsf{T}} + \boldsymbol{\nabla}\mathbf{u}^{\mathsf{T}}\boldsymbol{\nabla}\mathbf{u},$$
$$\mathbf{B} = \mathbf{F}\mathbf{F}^{\mathsf{T}} = \mathbf{I} + \boldsymbol{\nabla}\mathbf{u} + \boldsymbol{\nabla}\mathbf{u}^{\mathsf{T}} + \boldsymbol{\nabla}\mathbf{u}\boldsymbol{\nabla}\mathbf{u}^{\mathsf{T}}.$$

The Green-Lagrange strain tensor $\mathbf{E}$, is given by

$$\mathbf{E} = \frac{1}{2}\left(\mathbf{C} - \mathbf{I}\right) = \frac{1}{2}\left(\boldsymbol{\nabla}\mathbf{u} + \boldsymbol{\nabla}\mathbf{u}^{\mathsf{T}} + \boldsymbol{\nabla}\mathbf{u}^{\mathsf{T}}\boldsymbol{\nabla}\mathbf{u}\right).$$

Note that no approximations have been introduced in the kinematics as of yet and all the above equations are valid for non-linear elasticity.

2.1.3. Constitutive equations

In the previous section kinematics is briefly described. For brevity, the derivation of material and spatial, velocity and acceleration fields are omitted. The derivation of mass, linear momentum and angular momentum balance laws are also omitted. The reader is asked to refer Gurtin [19] for details on the same. In this work, we focus on static fields which basically means that all the fields are independent of time. Let us consider a body that occupies a region $\mathscr{B} \subset \mathscr{E}$ and has a motion subjected to an applied traction $\mathbf{s}$. Cauchy's theorem states that in such a scenario there exists a spatial second order tensor $\mathbf{T}$ called the Cauchy stress such that, for each unit vector $\mathbf{n}$, the following relation is satisfied,

$$\mathbf{s}(\mathbf{n}) = \mathbf{T}\mathbf{n},$$

and Cauchy stress $\mathbf{T} \in \mathrm{Sym}$. Further, $\mathbf{T}$ satisfies the equations of motion, which in the absence of body forces, for a static field is given as,

$$\mathrm{div}\ \mathbf{T} = 0,$$

which in the component form can be given as,

$$(\mathrm{div}\ \mathbf{T})_i = \frac{\partial T_{ij}}{\partial r_j},$$

where T_{ij} are the components of the $\mathbf{T}$ and r_j are the components of the spatial position vector $\mathbf{r}$ with respect to cartesian basis vectors. In finite elasticity, Cauchy stress tensor $\mathbf{T}(\mathbf{r})$ can be expressed in terms of deformation gradient $\mathbf{F}$ as follows,

$$\mathbf{T}(\mathbf{r}) = \hat{\mathbf{T}}\left(\mathbf{F}(\mathbf{R}), \mathbf{R}\right), \tag{4}$$ {T(F)}

where $\hat{\mathbf{T}} : \mathrm{Lin}^{+} \times \mathscr{B} \rightarrow \mathrm{Sym}$. Cauchy stress measures the surface force per unit area in the spatial configuration of the body. The first Piola-Kirchoff stress tensor is denoted by $\mathbf{P} : \mathscr{B} \times \mathbb{R} \rightarrow \mathrm{Lin}$ is the measure of surface force per unit are in the reference configuration. The relation between $\mathbf{T}$ and $\mathbf{P}$ is

$$\mathbf{P} = (\det \mathbf{F})\, \mathbf{T}\mathbf{F}^{-\mathrm{T}}.$$

Therefore, using the representation for $\mathbf{T}$ as a function of $\mathbf{F}$, we can conclude that $\mathbf{P} = \hat{\mathbf{P}}(\mathbf{F})$. The elasticity tensor $\mathsf{C} : \mathrm{Lin} \rightarrow \mathrm{Lin}$ is defined as,

$$\mathsf{C} := D\hat{\mathbf{P}}\,(\mathbf{I}) = D\hat{\mathbf{T}}\,(\mathbf{I})\,,$$

on the assumption,

es_stress}
$$\hat{\mathbf{P}}(\mathbf{I}) = \hat{\mathbf{T}}(\mathbf{I}) = 0 \tag{5}$$

Additonally, $\mathsf{C} \in \mathrm{PSym}$. The linearized version of elasticity is obtained by linearizing $\hat{\mathbf{S}}(\mathbf{F})$ about $\mathbf{I}$ as $\boldsymbol{\nabla}\mathbf{u} \rightarrow 0$. On substituting $\mathbf{F}$ from eq. (3) we get,

$$\mathbf{P} = \hat{\mathbf{P}}\,(\mathbf{I} + \boldsymbol{\nabla}\mathbf{u})\,.$$

On expanding $\hat{\mathbf{P}}$ about $\mathbf{I}$, using the assumption given in eq. (5) and using the symmetric properties of C we get,

$$\hat{\mathbf{P}} = \mathsf{C}[\boldsymbol{\epsilon}] + o\,(\boldsymbol{\nabla}\mathbf{u})\,, \tag{6}$$

where $\boldsymbol{\epsilon}$ is the linearized or infinitesimal strain tensor,

{strain}
$$\boldsymbol{\epsilon} = \frac{1}{2}\left(\boldsymbol{\nabla}\mathbf{u} + \boldsymbol{\nabla}\mathbf{u}^{\mathsf{T}}\right), \tag{7}$$

In the limit $\boldsymbol{\nabla}\mathbf{u} \rightarrow 0$, the deformed and reference configurations can be considered to be almost identical and therefore, $\hat{\mathbf{T}} = \hat{\mathbf{P}}$. Hence, the Cauchy stress tensor is,

$$\mathbf{T} = \mathsf{C}[\boldsymbol{\epsilon}] = 2\mu\boldsymbol{\epsilon} + \lambda(\mathrm{tr}\ \boldsymbol{\epsilon})\mathbf{I},$$

as $\boldsymbol{\nabla}\mathbf{u} \rightarrow 0$. The symbols μ and λ are material parameters commonly referred to as Lame's parameters. Since, we are considering the linearized version of elasticity the Cauchy stress will be denoted by $\boldsymbol{\tau}$ in the rest of the work. In the presence of thermo-elastic strain (residual strain) $\boldsymbol{\epsilon}_0$, the constitutive equations are expressed as,

{Cauchy1}
$$\boldsymbol{\tau} = \mathsf{C}[\boldsymbol{\epsilon} - \boldsymbol{\epsilon}_0] = 2\mu\,(\boldsymbol{\epsilon} - \boldsymbol{\epsilon}_0) + \lambda(\mathrm{tr}\,(\boldsymbol{\epsilon} - \boldsymbol{\epsilon}_0))\,\mathbf{I}, \tag{8}$$

and $\boldsymbol{\epsilon} - \boldsymbol{\epsilon}_0$ is commonly referred to as elastic strain, (see xyz for details).

3. Helical coordinate system

As mentioned in the introduction, we formulate the linear thermo-elastic boundary value problem in curvilinear coordinates. Therefore, we introduce curvilinear coordinate theory from Green and Zerna (see [21]) that is necessary to express linear thermo-elasticity in helical co-ordinates. Let $\{x^1, x^2, x^3\} \in \mathscr{E}$ be the regular right-handed orthogonal cartesian co-ordinate system and can be seen in Fig. 2. Curvilinear coordinates θ^i can be introduced by a transformation as given in [21], as follows,

{thetatox}
$$\theta^i = \theta^i(x^1, x^2, x^3). \tag{9}$$

It is assumed that this transformation is invertible as long as the constraint $\det\left[\partial x^i/\partial\theta^j\right] \neq 0$ holds .i.e., x^i can be expressed in terms of θ^i. Therefore, we get

$$x^i = x^i(\theta^1, \theta^2, \theta^3). \tag{10}$$ {xtotheta

A schematic of the transformation is shown in Fig. 2, where a position vector $\mathbf{R}$ of a point $\mathcal{P} \in \mathscr{E}$ is expressed in curvilinear coordinates $\{\theta^1, \theta^2, \theta^3\}$. The equation $\theta^i(x^1, x^2, x^3)$ equal to a constant represents three surfaces corresponding $i = 1, 2, 3$. For example, in Fig. 2, θ^3 = constant is a surface with θ^1, θ^2 varying spatially. Further, intersection of these surfaces at the point $\mathcal{P}$ gives us three curves called the coordinate curves.

To understand helical symmetry, we introduce a specific curvilinear coordinate system identical to the one introduced by Overfelt (see [22]) for helical harmonics. Let $\{\theta^1, \theta^2, \theta^3\}$, be given as,

$$\theta^1 = \rho, \theta^2 = \phi \text{ and } \theta^3 = \zeta, \tag{11}$$ {thetadef

then the transformation between cartesian and helical coordinate system can be defined as follows, {helical_

$$x^1 := \rho\cos(\phi), \tag{12a}$$
$$x^2 := \rho\sin(\phi), \tag{12b}$$
$$x^3 := \bar{L}\,\phi + \zeta, \tag{12c}$$

where, $\bar{L} = L/2\pi$, and $\bar{L}$ is the pitch of the helix. The coordinate system is illustrated in Fig. 3, where the helix are plotted using the above mentioned transformation between cartesian and helical coordinates. The coordinate curve ρ varies from a to b, where $a, b \in \mathbb{R}^+$ and a and b are called as the inner and outer radius of the helix, respectively. The coordinate ϕ varies along the helix as seen and *zeta* varies along the pitch of the helix. On comparing the helical coordinates to the cylindrical coordinates $\{r, \theta, z\}$, we see that $\theta \in [0, 2\pi)$ and $z \in (-\infty, \infty)$ whereas $\phi \in (-\infty, \infty)$ and $\zeta \in [-L/2, L/2)$. Further, $r \in (0, \infty)$ and $\rho \in (0, \infty)$ and the mapping between cylindrical and helical coordinates is one-to-one except at $\rho = r = 0$. Similarly, the

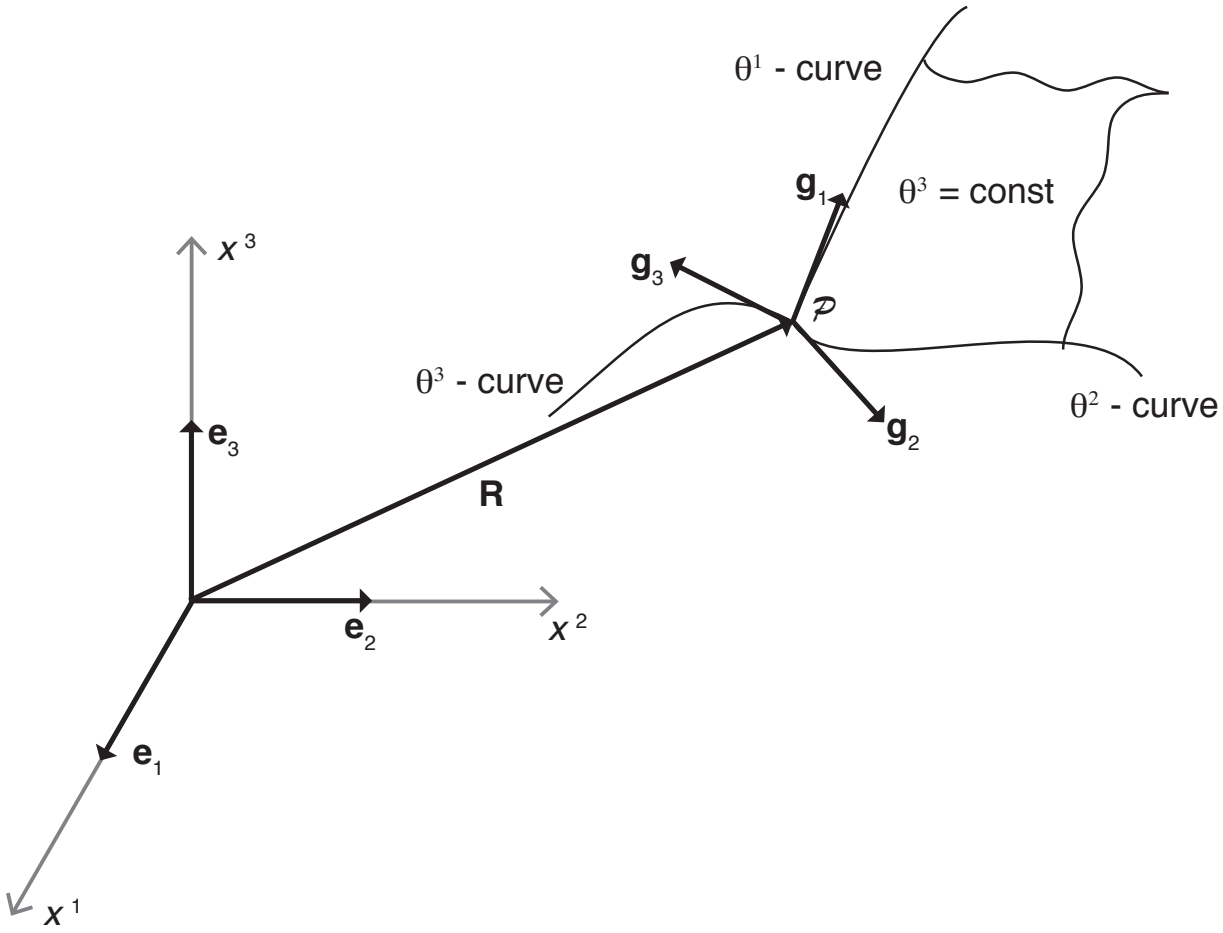

Figure 2: In this figure, the transformation between the cartesian coordinate system $\{x^1, x^2, x^3\}$ and a curvilinear coordinate system $\{\theta^1, \theta^2, \theta^3\}$. The position vector of point $\mathcal{P}$ is denoted by $\mathbf{R}$. The cartesian basis vectors are given as $\{\mathbf{e}_1, \mathbf{e}_2, \mathbf{e}_3\}$, while the covariant basis vectors are given as $\{\mathbf{g}_1, \mathbf{g}_2, \mathbf{g}_3\}$.

{coor}

helical coordinates $\{\rho, \phi, \zeta\}$ can be expressed in terms of $\{x^1, x^2, x^3\}$ as follows,

{helical_c

$$\rho = \sqrt{(x^1)^2 + (x^2)^2}, \tag{13a}$$

$$\phi = \arctan\left(\frac{x^2}{x^1}\right), \tag{13b}$$

$$\zeta = x^3 - \bar{L}\ \arctan\left(\frac{x^2}{x^1}\right). \tag{13c}$$

3.1. Covariant and Contravariant basis vectors

To derive the basis vectors for the helical coordinate system let us define the position vector $\mathbf{R}$ to be,

$$\mathbf{R} := x^1\ \mathbf{e}_1 + x^2\ \mathbf{e}_2 + x^3\ \mathbf{e}_3,$$

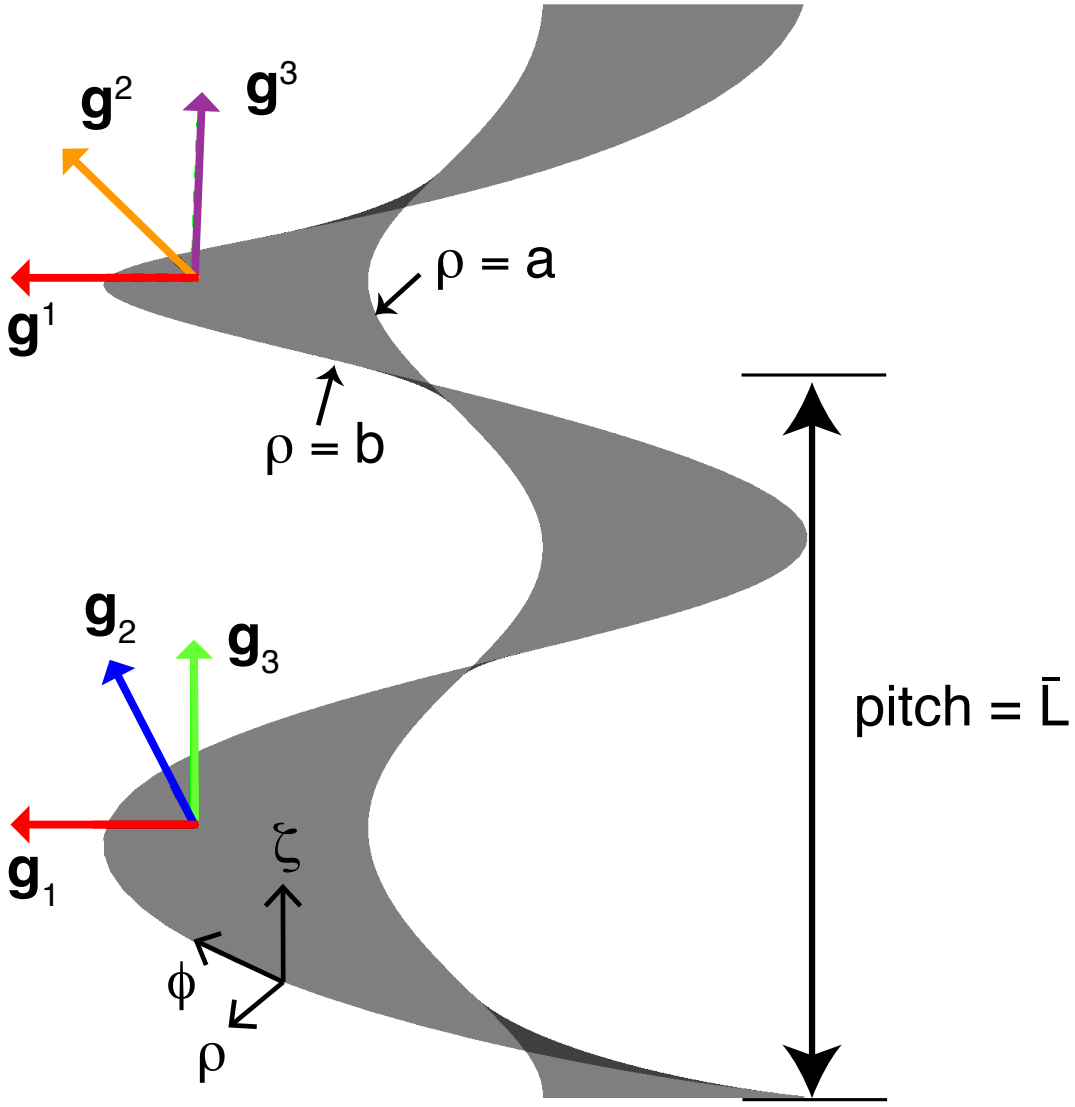

Figure 3: In this figure a schematic of the helix is shown where the helical coordinates $\{\rho, \phi, \zeta\}$ are shown. The coordinate ρ varies from a to b, where $\rho = a$ and $\rho = b$ are marked in the figure. The pitch of the helix $\bar{L}$ is also indicated in the figure. The covariant basis vectors, i.e., $\{\mathbf{g}_1, \mathbf{g}_2, \mathbf{g}_3\}$ are shown using red, blue and green arrows. Similarly, the contravariant basis vectors, i.e., $\{\mathbf{g}^1, \mathbf{g}^2, \mathbf{g}^3\}$ are shown using red, orange and magenta arrows. Since $\mathbf{g}_1 = \mathbf{g}^1$, red color arrows are used to indicate that they are identical.

basis_vec}

where, $\mathbf{e}_1,\ \mathbf{e}_2$ and $\mathbf{e}_3 = (0,0,1)$ are linearly independent orthogonal unit basis vectors in $\mathbb{R}^3$ mentioned in section 1.1.1 which are commonly known as the cartesian basis vectors. Further, $\{x^1, x^2, x^3\}$ are the components of the position vector $\mathbf{R}$ in $\{\mathbf{e}_1, \mathbf{e}_2, \mathbf{e}_3\}$ basis. We can express $\mathbf{R}$ in terms of $\{\rho, \phi, \zeta\}$ on substituting $\{x^1, x^2, x^3\}$ from eq. (12) and we obtain,

{pos_vec}

$$\mathbf{R} = \rho\cos(\phi)\ \mathbf{e}_1 + \rho\sin(\phi)\ \mathbf{e}_2 + (\bar{L}\,\phi + \zeta)\ \mathbf{e}_3. \tag{14}$$

The covariant basis vectors $\{\mathbf{g}_1, \mathbf{g}_2, \mathbf{g}_3\}$ are tangent vectors to the coordinate curves $\{\rho, \phi, \zeta\}$ at $\mathbf{R}$, respectively, and are illustrated in Fig. 3. They are defined as given in [21] as,

vec_cart}

$$\mathbf{g}_1 := \frac{\partial x^j}{\partial \rho}\ \mathbf{e}_j = \cos(\phi)\ \mathbf{e}_1 + \sin(\phi)\ \mathbf{e}_2, \tag{15a}$$

$$\mathbf{g}_2 := \frac{\partial x^j}{\partial \phi}\ \mathbf{e}_j = -\rho\sin(\phi)\ \mathbf{e}_1 + \rho\cos(\phi)\ \mathbf{e}_2 + \bar{L}\ \mathbf{e}_3, \tag{15b}$$

$$\mathbf{g}_3 := \frac{\partial x^j}{\partial \zeta}\ \mathbf{e}_j = \mathbf{e}_3. \tag{15c}$$

The short hand or indicial notation reads as $\mathbf{g}_i := \partial x^j/\partial\theta^i\ \mathbf{e}_j$. Similarly, the contravariant basis vectors are denoted using superscripts and are defined as $\mathbf{g}^i := \partial\theta^i/\partial x^j\ \mathbf{e}_j$. We can express $\{\theta^1, \theta^2, \theta^3\}$ in terms of $\{x^1, x^2, x^3\}$ from eq. (13) and compute the contravariant basis vectors as,

vec_cart}

$$\mathbf{g}^1 := \frac{\partial \rho}{\partial x^j}\ \mathbf{e}_j = \cos(\phi)\ \mathbf{e}_1 + \sin(\phi)\ \mathbf{e}_2 \tag{16a}$$

$$\mathbf{g}^2 := \frac{\partial \phi}{\partial x^j}\ \mathbf{e}_j = \frac{1}{\rho}\left(-\sin(\phi)\ \mathbf{e}_1 + \cos(\phi)\ \mathbf{e}_2\right), \tag{16b}$$

$$\mathbf{g}^3 := \frac{\partial \zeta}{\partial x^j}\ \mathbf{e}_j = \frac{-\bar{L}}{\rho}\left(-\sin(\phi)\ \mathbf{e}_1 + \cos(\phi)\ \mathbf{e}_2\right) +\ \mathbf{e}_3. \tag{16c}$$

The contravariant vectors are $\{\mathbf{g}^1, \mathbf{g}^2, \mathbf{g}^3\}$ are orthogonal to $\{\rho, \phi, \zeta\}$ coordinate planes, respectively. For example, $\mathbf{g}^1$ is normal to the plane ρ = constant. The covariant basis vectors can be

r_vec_cyl}

expressed in cylindrical basis vectors as follows:

$$\mathbf{g}_1 = \mathbf{e}_r, \tag{17a}$$

$$\mathbf{g}_2 = \rho\ \mathbf{e}_\theta + \bar{L}\ \mathbf{e}_z, \tag{17b}$$

$$\mathbf{g}_3 = \mathbf{e}_z, \tag{17c}$$

where $\mathbf{e}_r,\ \mathbf{e}_\theta,\ \mathbf{e}_z$ are the cylindrical basis vectors (see [21] for details). Similarly, the contravari-

r_vec_cyl}

ant basis vectors in cylindrical basis vectors are,

$$\mathbf{g}^1 = \mathbf{e}_r \tag{18a}$$

$$\mathbf{g}^2 = \frac{1}{\rho}\ \mathbf{e}_\theta \tag{18b}$$

$$\mathbf{g}^3 = -\frac{\bar{L}}{\rho}\ \mathbf{e}_\theta + \mathbf{e}_z. \tag{18c}$$

3.2. Metric tensors

The covariant and contravariant metric tensors in the component for are defined as,

$$g_{ij} = \frac{\partial x^m}{\partial \theta^i}\frac{\partial x^m}{\partial \theta^j}, \tag{19a}$$

$$g^{ij} = \frac{\partial \theta^i}{\partial x^m}\frac{\partial \theta^j}{\partial x^m}, \tag{19b}$$

respectively. Therefore, on substituting the x^i in terms of θ^i from eq. 12 we can evaluate the covariant metric tensor g_{ij}. Similarly, on substituting the θ^i in terms of x^i from eq. 13 we can evaluate the contravariant metric tensor g^{ij}. The metric tensors for the helical coordinates are,

$$g_{ij} = \begin{bmatrix} 1 & 0 & 0 \\ 0 & \rho^2 + \bar{L}^2 & \bar{L} \\ 0 & \bar{L} & 1 \end{bmatrix}. \tag{20}$$

Similarly, the contravariant metric tensor can be evaluated to be,

$$g^{ij} = \begin{bmatrix} 1 & 0 & 0 \\ 0 & \frac{1}{\rho^2} & -\frac{\bar{L}}{\rho^2} \\ 0 & -\frac{\bar{L}}{\rho^2} & \frac{\bar{L}^2+\rho^2}{\rho^2} \end{bmatrix}. \tag{21}$$

3.3. Surface area and volume

The infinitesimal line elements along coordinate curves $\{\theta^1, \theta^2, \theta^3\}$ can be represented by vectors as,

$$d\mathbf{s}_1 = \mathbf{g}_1\, d\theta^1, \tag{22a}$$

$$d\mathbf{s}_2 = \mathbf{g}_2\, d\theta^2, \tag{22b}$$

$$d\mathbf{s}_3 = \mathbf{g}_3\, d\theta^3. \tag{22c}$$

The infinitesimal volume element dV enclosed by these line elements can be defined and simplified using the line element equations as,

$$\begin{aligned} dV &:= d\mathbf{s}_1 \cdot (d\mathbf{s}_2 \times d\mathbf{s}_3)\,, \\ &= \mathbf{g}_1 \cdot (\mathbf{g}_2 \times \mathbf{g}_3)\; d\theta^1\, d\theta^2\, d\theta^3, \end{aligned}$$

where $(\cdot)$ indicates the scalar dot product and $(\times)$ the cross product (not defined). The scalar $\mathbf{g}_1 \cdot (\mathbf{g}_2 \times \mathbf{g}_3)$ can be expressed as $[\mathbf{g}_1\ \mathbf{g}_2\ \mathbf{g}_3]$ which is the scalar dot product of three vectors. It has been shown in Green and Zerna [21], that $[\mathbf{g}_1\ \mathbf{g}_2\ \mathbf{g}_3] = \sqrt{\det[g_{ij}]}$

$$dV = \sqrt{\det\left[g_{ij}\right]}\, d\theta^1\, d\theta^2\, d\theta^3.$$

The determinant of g_{ij} from eq. (20) is evaluated to be ρ^2 and substituting it in the above equation we get dV to be,

$$dV = \rho\, d\rho\, d\phi\, d\zeta. \tag{23}$$

It is a mere coincidence that the differential volume in this case is identical to the one in cylindrical co-ordinate system. In order to compute the total volume of the helix, the domain of the helix is defined in terms of dimensionless variables as,

$$\mathscr{B} := \left\{(\hat{\rho}, \phi, \hat{\zeta}) \ : \ \hat{\rho} \in [1, \hat{b}],\ \phi \in [0, 2\pi),\ \hat{\zeta} \in (-\pi\hat{L}, \pi\hat{L})\right\}, \tag{24}$$ {Omega}

where $\hat{\rho} = \rho/a$, $\hat{\zeta} = \zeta/a$. The inner radius $a \in \mathbb{R}^+$ and outer radius $b \in \mathbb{R}^+$ of the helix should satisfy the constraint that the dimensionless outer radius $\hat{b} = b/a > 1$. The symbol $\hat{L} \in \mathbb{R}^+$ is related to the pitch of the helix $\bar{L}$ as $\bar{L} = a\hat{L}$. We introduce the non-dimensional total volume $\hat{V} = V/a^3$, which can be computed as follows,

{volume}
$$\begin{aligned} \hat{V} &= \int_{\mathscr{B}} \hat{\rho}\, d\hat{\rho}\, d\phi\, d\hat{\zeta} = \int_{-\pi\hat{L}}^{\pi\hat{L}} \int_0^{2\pi} \int_1^{\hat{b}} \hat{\rho}\, d\hat{\rho}\, d\phi\, d\hat{\zeta}, \\ &= 2\pi^2 \left(\hat{b}^2 - 1\right) \hat{L}. \end{aligned} \tag{25}$$

Similarly, the infinitesimal helicoidal surface area element denoted by $d\mathbf{A}$ is defined as,

$$d\mathbf{A} := (d\mathbf{s}_1 \times d\mathbf{s}_2)\ d\theta^1\ d\theta^2.$$

Using the definition for the line elements given in eq. (22) and expressing $\mathbf{g}_1$, $\mathbf{g}_2$ in terms of the cylindrical basis vectors given in eq. (17) we get infinitesimal area vector to be,

$$\begin{aligned} d\mathbf{A} &= (\mathbf{g}_1 \times \mathbf{g}_2)\ d\rho\, d\phi, \\ &= \left(-\bar{L}\, \mathbf{e}_\theta + \rho\, \mathbf{e}_z\right)\ d\rho\, d\phi. \end{aligned}$$

Using the definition of magnitude of a vector given in eq. (1), the magnitude of the area element can be evaluated to be

face_area}
$$|d\mathbf{A}| = \sqrt{\bar{L}^2 + \rho^2}\ d\rho\, d\phi, \tag{26}$$

where, $|\cdot|$ denotes the magnitude of a vector given in eq. (1). The total surface area is given as,

$$A = \int_0^{2\pi} \int_a^b |d\mathbf{A}|, \tag{27}$$

We introduce $\hat{A} = A/\pi a^2$. Thus, in dimensionless form,

coid_area}
$$\hat{A} = \hat{b}\sqrt{\hat{b}^2 + \hat{L}^2} - \sqrt{1 + \hat{L}^2} + \hat{L}^2 \log\left[\frac{\hat{b} + \sqrt{\hat{b}^2 + \hat{L}^2}}{1 + \sqrt{1 + \hat{L}^2}}\right] \tag{28}$$

Further, the non-dimensional helicoidal surface area $\hat{A}$ in the limit of $\hat{L} \to 0$, gives the non-dimensional area of the circular annulus, i.e., $\hat{b}^2 - 1$, which is consistent with the theory that as $\hat{L} \to 0$, the helical coordinates reduce to cylindrical coordinates.

3.4. Christoffel symbols of the second kind

Gradient and divergence of a tensor are expressed in terms of Christoffel symbols. The Christoffel symbols of the second kind in the component form is,

$$\Gamma^k_{ij} = g^{ks}\,\frac{\partial^2 x^r}{\partial\theta^i\partial\theta^j}\frac{\partial x^r}{\partial\theta^s},$$

respectively. Therefore, on substituting θ^i from eq. (11) and x^i from eq. (12), we obtain Christoffel symbols of the second kind for the helical coordinates to be,

$$\begin{aligned}\Gamma^1_{22} &= \rho,\\ \Gamma^2_{12} = \Gamma^2_{21} &= \frac{1}{\rho},\\ \Gamma^3_{12} = \Gamma^3_{21} &= \frac{-\bar{L}}{\rho},\end{aligned} \tag{29}$$ {Christof

and all other components of $\Gamma^k_{ij} = 0$.

3.5. Scalar product and cross product of vectors

Let us define some preliminary mathematical operators in cruvilinear coordinates that would be used extensively in the later sections. The kronecker delta in curvilinear coordinates is defined as, {kronecke

$$\delta_{ij} = \delta^{ij} = \delta^i_j = \delta^j_i = 0\ (i \neq j), \tag{30a}$$

$$\delta_{ij} = \delta^{ij} = \delta^i_j = \delta^j_i = 0\ (i = j,\ j \text{ not summed}). \tag{30b}$$

From the definition of metric tensors given in eq. 19, we can see that

$$g_{im}\ g^{mj} = \delta^j_i, \tag{31}$$

A vector $\mathbf{u}$ can be expressed using the covariant $\{\mathbf{g}_1,\ \mathbf{g}_2,\ \mathbf{g}_3\}$ and contravariant basis vectors $\{\mathbf{g}^1,\ \mathbf{g}^2,\ \mathbf{g}^3\}$ as follows,

$$\mathbf{u} = u_i\ \mathbf{g}^i = u^i\ \mathbf{g}_i, \tag{32}$$ {vector}

where u_i and u^i are the covariant and contravariant components, respectively. The relation between the respective components can be expressed as follows, {covar_co

$$u^i = g^{ik}\ u_k, \tag{33a}$$

$$u_i = g_{ik}\ u^k. \tag{33b}$$

A second order tensor $\mathbf{A}$ can be represented as, {tensor}

$$\begin{aligned}\mathbf{A} &= A_{ij}\ \mathbf{g}^i \otimes \mathbf{g}^j, &(34a)\\ &= A^{ij}\ \mathbf{g}_i \otimes \mathbf{g}_j, &(34b)\\ &= A^i_{\cdot j}\ \mathbf{g}_i \otimes \mathbf{g}^j, &(34c)\\ &= A^{\cdot j}_i\ \mathbf{g}^i \otimes \mathbf{g}_j, &(34d)\end{aligned}$$

where A_{ij}, A^{ij} are the covariant and contravariant components of $\mathbf{A}$. Further, if $\mathbf{A} \in \mathrm{Sym}$ then the components satisfy, $A_{ij} = A_{ji}$ and $A^{ij} = A^{ji}$. The symbols $A^{i}_{\cdot j}$ and $A^{\cdot j}_{i}$ are the mixed components of $\mathbf{A}$ and satisfy the relation $A^{i}_{\cdot j} = A^{\cdot i}_{j}$ if $\mathbf{A} \in \mathrm{Sym}$. The scalar product for two vectors $\mathbf{u}$ and $\mathbf{v}$ is denoted by $\mathbf{u} \cdot \mathbf{v}$ and is defined as,

t_product}

$$\mathbf{u} \cdot \mathbf{v} = u_i \, v^i = u^i \, v_i. \tag{35}$$

The inner product of a vector $\mathbf{u}$ denoted by $|\mathbf{u}|$ is,

$$|\mathbf{u}| = (\mathbf{u} \cdot \mathbf{u})^{1/2} = \left(u^i \, u_i\right)^{1/2}. \tag{36}$$

The tensor product of two vectors $\mathbf{u}$ and $\mathbf{v}$ denoted by $\mathbf{u} \otimes \mathbf{v}$ is given as,

$$\mathbf{u} \otimes \mathbf{v} = u_i \, v_j \, \mathbf{g}^i \otimes \mathbf{g}^j, \tag{37a}$$
$$= u^i \, v^j \, \mathbf{g}_i \otimes \mathbf{g}_j, \tag{37b}$$
$$= u_i \, v^j \, \mathbf{g}^i \otimes \mathbf{g}_j, \tag{37c}$$
$$= u^i \, v_j \, \mathbf{g}_i \otimes \mathbf{g}^j. \tag{37d}$$

{misc} Further, some of the other important identities are

$$g_{ij} = \mathbf{g}_i \cdot \mathbf{g}_j, \tag{38a}$$
$$g^{ij} = \mathbf{g}^i \cdot \mathbf{g}^j, \tag{38b}$$
$$\mathbf{g}^i \cdot \mathbf{g}_j = \delta^i_j. \tag{38c}$$

tor_cross} Finally, the scalar triple product is given as,

$$\sqrt{\det\left[g_{ij}\right]} = \mathbf{g}_1 \cdot (\mathbf{g}_2 \times \mathbf{g}_3), \tag{39a}$$
$$\sqrt{\det\left[g^{ij}\right]^{-1}} = \mathbf{g}^1 \cdot \left(\mathbf{g}^2 \times \mathbf{g}^3\right). \tag{39b}$$

3.6. Gradient and divergence in curvilinear coordinates

Let us consider a vector $\mathbf{v} = v_i \, \mathbf{g}^i$, where v_i are the covariant components of the vector.

{grad} The gradient of vector $\mathbf{v}$ can be defined as follows,

$$\boldsymbol{\nabla}\mathbf{v} = v_i|_j \, \mathbf{g}^i \otimes \mathbf{g}^j, \tag{40a}$$

where,

$$v_i|_j = \frac{\partial v_i}{\partial \theta^j} - \Gamma^k_{ij} \, v_k. \tag{40b}$$

Let us consider a second order tensor $\mathbf{A} = A^{ij} \, \mathbf{g}_i \otimes \mathbf{g}_j$, where A^{ij} are the contravariant compo-

{div} nents of $\mathbf{A}$, the divergence of $\mathbf{A}$ can be expressed as,

$$\mathrm{div}\ \mathbf{A} = A^{ij}|_j \, \mathbf{g}_i, \tag{41a}$$

where,

$$A^{ij}|_j = \frac{\partial A^{ij}}{\partial \theta^j} + \Gamma^i_{mj} \, A^{mj} + \Gamma^j_{mj} \, A^{im}. \tag{41b}$$

3.7. Constitutive equations specialized to helical coordinates

The displacement $\mathbf{u}$ is expressed in terms of contravariant components $\mathbf{u} = u^i\ \mathbf{g}_i$. The covariant components can be simply obtained by using transformation given in eq. (33). The strain tensor $\boldsymbol{\epsilon}$ defined in eq. (7) can be expressed in helical coordinates on using the definition of $\boldsymbol{\nabla}\mathbf{u}$ given in eq. (40),

$$\boldsymbol{\epsilon} = \frac{1}{2}\left(u_i|_j + u_j|_i\right)\ \mathbf{g}^i \otimes \mathbf{g}^j. \tag{42}$$ {strain_he

Let the strain tensor be $\boldsymbol{\epsilon} = \epsilon_{ij}\ \mathbf{g}^i \otimes \mathbf{g}^j$, where ϵ_{ij} are the covariant components of the strain tensor. We can simplify the above equation using eq. (40), and ϵ_{ij} is given as,

$$\epsilon_{ij} = \frac{1}{2}\left(\frac{\partial u_i}{\partial \theta^j} + \frac{\partial u_j}{\partial \theta^i} - \Gamma^k_{ij}u_k - \Gamma^k_{ji}u_k\right). \tag{43}$$ {strain_co

The thermal strain coming from a prescribed temperature distribution $\Delta T : \mathscr{B} \to \mathbb{R}$, is given as,

$$\boldsymbol{\epsilon}_0 = \alpha\ \Delta T\ \mathbf{I},$$

where $\alpha \in \mathbb{R}^+$ is the thermal expansion coefficient. The Cauchy stress tensor $\boldsymbol{\tau}$ given in eq. (8) is expressed in helical coordinates as,

$$\begin{aligned} \boldsymbol{\tau} &= \mathsf{C}^{ijrs}\ \left(\epsilon_{rs} - \epsilon_{0rs}\right)\ \mathbf{g}_i \otimes \mathbf{g}_j, \\ \tau^{ij} &= \mathsf{C}^{ijrs}\left(\epsilon_{rs} - \epsilon_{0rs}\right), \end{aligned} \tag{44}$$ {cauchystr

in tensor and component form, respectively. The elasticity tensor C in component form is,

$$\mathsf{C}^{ijrs} = \mu\ \left(g^{ir}g^{js} + g^{is}g^{jr}\right) + \lambda\ g^{ij}g^{rs}. \tag{45}$$ {Cijkl}

The strain energy density is defined as,

$$W = \frac{1}{2}\boldsymbol{\tau} : \boldsymbol{\epsilon}.$$

It can expressed in component form using the definition of strain and stress from eq. (7) and (44), respectively, and the properties of Kronecker delta given in eq. (30) and (38),

$$\begin{aligned} W &= \frac{1}{2}\left(\tau^{ij}\ \mathbf{g}_i \otimes \mathbf{g}_j\right) : \left(\epsilon_{kl}\ \mathbf{g}^k \otimes \mathbf{g}^l\right), \\ &= \frac{1}{2}\tau^{ij}\ \epsilon_{kl}\left(\mathbf{g}_i \cdot \mathbf{g}^k\right)\left(\mathbf{g}_j \cdot \mathbf{g}^l\right) \\ &= \frac{1}{2}\tau^{ij}\ \epsilon_{kl}\left(\mathbf{g}_i \cdot \mathbf{g}^k\right)\left(\mathbf{g}_j \cdot \mathbf{g}^l\right) \\ &= \frac{1}{2}\tau^{ij}\ \epsilon_{kl}\ \delta^k_i\ \delta^l_j \\ &= \frac{1}{2}\tau^{ij}\ \epsilon_{ij}. \end{aligned} \tag{46}$$ {enden}

Similarly, the elastic strain energy density is given as,

$$W^e = \frac{1}{2}\tau^{ij}\,\left(\epsilon_{ij} - \epsilon_{0ij}\right). \tag{47}$$ {elastic_

The total elastic strain energy Π^e and strain energy Π is defined as $\int_{\mathscr{B}} W^e dV$ and $\int_{\mathscr{B}} W dV$, respectively, where $\mathscr{B}$ is the periodic segment of the helicoid given in eq. (24). The expressions for Π^e and Π can simplified using the definition of dV from eq. (23), and are given as,

{pi}
$$\Pi = \int_{-L/2}^{L/2}\int_{0}^{2\pi}\int_{a}^{b} W\,\rho\,d\rho\,d\phi\,d\zeta, \tag{48a}$$

{pie}
$$\Pi^e = \int_{-L/2}^{L/2}\int_{0}^{2\pi}\int_{a}^{b} W^e\,\rho\,d\rho\,d\phi\,d\zeta. \tag{48b}$$

Finally, we can express the equilibrium equations in helical coordinates using eq. (41),

uilibrium}
$$\operatorname{div}\boldsymbol{\tau} = \tau^{ij}|_j\,\mathbf{g}_i, \tag{49}$$

where,

$$\tau^{ij}|_j = \frac{\partial\tau^{ij}}{\partial\theta^j} + \Gamma^i_{mj}\,\tau^{mj} + \Gamma^j_{mj}\,\tau^{im}.$$

3.8. Traction vector

We can denote the work done by applied traction as P_{ext} on boundary $\partial\mathscr{B}$ and can be simplified as follows,

$$\begin{aligned}
\mathrm{P}_{\text{ext}} &= \int_{\partial\mathscr{B}} \mathbf{t}\cdot\mathbf{u}\,dA,\\
&= \int_{\partial\mathscr{B}} t_i\,\mathbf{g}^i\cdot u^k\,\mathbf{g}_k\,dA,\\
&= \int_{\partial\mathscr{B}} t_i\,u^k\,\delta^i_k\,dA,\\
&= \int_{\partial\mathscr{B}} t_i\,u^i\,dA.
\end{aligned}$$

The traction vector is defined as $\mathbf{t} = \boldsymbol{\tau}\cdot\mathbf{n}$, where $\mathbf{n}$ is unit normal vector to the boundary. By definition of contravariant vectors, $\mathbf{g}^i$ the normal vector $\mathbf{n} = \pm\mathbf{g}^i/|\mathbf{g}^i|$. A schematic of the domain in $\{\rho,\zeta\}$ coordinate system is shown in Fig. 4. The boundaries can be defined as,

[zetaboun}
$$\partial\mathscr{B}_1 = \left\{(\hat{\rho},\phi,\hat{\zeta})\ :\ \hat{\rho}\in[1,\hat{b}],\ \phi\in[0,2\pi),\ \hat{\zeta} = \pi\hat{L}\right\}, \tag{50a}$$

$$\partial\mathscr{B}_2 = \left\{(\hat{\rho},\phi,\hat{\zeta})\ :\ \hat{\rho}\in[1,\hat{b}],\ \phi\in[0,2\pi),\ \hat{\zeta} = -\pi\hat{L}\right\}. \tag{50b}$$

From the schematic in Fig. 4, it can be seen that the unit normal vectors to $\partial\mathscr{B}_1$ and $\partial\mathscr{B}_2$, are
{rhoboun} $\mathbf{g}^3/|\mathbf{g}^3|$ and $-\mathbf{g}^3/|\mathbf{g}^3|$, respectively. Similarly, the other two boundaries can identified as,

$$\partial\mathscr{B}_3 = \left\{(\hat{\rho},\phi,\hat{\zeta}) \ : \ \hat{\rho}=1,\ \phi\in[0,2\pi),\ \hat{\zeta}\in(-\pi\hat{L},\pi\hat{L})\right\}, \tag{51a}$$

$$\partial\mathscr{B}_4 = \left\{(\hat{\rho},\phi,\hat{\zeta}) \ : \ \hat{\rho}=\hat{b},\ \phi\in[0,2\pi),\ \hat{\zeta}\in(-\pi\hat{L},\pi\hat{L})\right\}, \tag{51b}$$

where the normal to the boundary at $\partial\mathscr{B}_3$ is $-\mathbf{g}^1/|\mathbf{g}^1|$ and at $\partial\mathscr{B}_4$ is $\mathbf{g}^1/|\mathbf{g}^1|$. The traction components t_i in terms of components of $\boldsymbol{\tau}$ is given as,

$$\begin{aligned}
\mathbf{t} &= \boldsymbol{\tau}\cdot\mathbf{n},\\
t_i\,\mathbf{g}^i &= \tau_i^{\cdot j}\left(\mathbf{g}^i\otimes\mathbf{g}_j\right)\cdot\frac{\pm\mathbf{g}^k}{|\mathbf{g}^k|},\\
&= \pm\tau_i^{\cdot j}\left(\mathbf{g}_j\cdot\frac{\mathbf{g}^k}{|\mathbf{g}^k|}\right)\mathbf{g}^i,\\
&= \pm\tau_i^{\cdot j}\delta_j^k\frac{\mathbf{g}^i}{|\mathbf{g}^k|},\\
&= \pm\tau_i^{\cdot k}\frac{\mathbf{g}^i}{|\mathbf{g}^k|},\\
t_i &= \pm\frac{\tau_i^{\cdot k}}{|\mathbf{g}^k|}.
\end{aligned} \tag{52}$$

{traction}

Therefore, the traction vectors at the different boundaries are,

{trac_com

$$\mathbf{t} = \frac{1}{|\mathbf{g}^3|}\left(\tau_1^{\cdot 3}\mathbf{g}^1+\tau_2^{\cdot 3}\mathbf{g}^2+\tau_3^{\cdot 3}\mathbf{g}^3\right)\ \text{on}\ \partial\mathscr{B}_1, \tag{53a}$$

$$= -\frac{1}{|\mathbf{g}^3|}\left(\tau_1^{\cdot 3}\mathbf{g}^1+\tau_2^{\cdot 3}\mathbf{g}^2+\tau_3^{\cdot 3}\mathbf{g}^3\right)\ \text{on}\ \partial\mathscr{B}_2, \tag{53b}$$

$$= -\frac{1}{|\mathbf{g}^1|}\left(\tau_1^{\cdot 1}\mathbf{g}^1+\tau_2^{\cdot 1}\mathbf{g}^2+\tau_3^{\cdot 1}\mathbf{g}^3\right)\ \text{on}\ \partial\mathscr{B}_3, \tag{53c}$$

$$= \frac{1}{|\mathbf{g}^1|}\left(\tau_1^{\cdot 1}\mathbf{g}^1+\tau_2^{\cdot 1}\mathbf{g}^2+\tau_3^{\cdot 1}\mathbf{g}^3\right)\ \text{on}\ \partial\mathscr{B}_4. \tag{53d}$$

3.9. Helical symmetry

{helical_

Helical symmetry is present, if none of the fields change as we move along a helical material fiber of pitch $\hat{L}$. If we hold $\hat{\zeta}$ and $\hat{\rho}$ and vary ϕ, we move along a helical material fiber of pitch L; each pair of co-ordinates $(\hat{\rho},\hat{\zeta})$ define a helical material fiber in the cylinder. Therefore, in our current problem all the fields should depend only on $(\hat{\rho},\hat{\zeta})$. Therefore, helical symmetry indicates that the linear elastic equilibrium equations do not depend on the helical coordinate ϕ. This can be understood by considering the analogy of the axisymmetric case in cylindrical coordinates, where the equilibrium equations in cylindrical coordinates do not depend on θ. Therefore, we can expand the equilibrium equations in eq. (49) using the assumption that

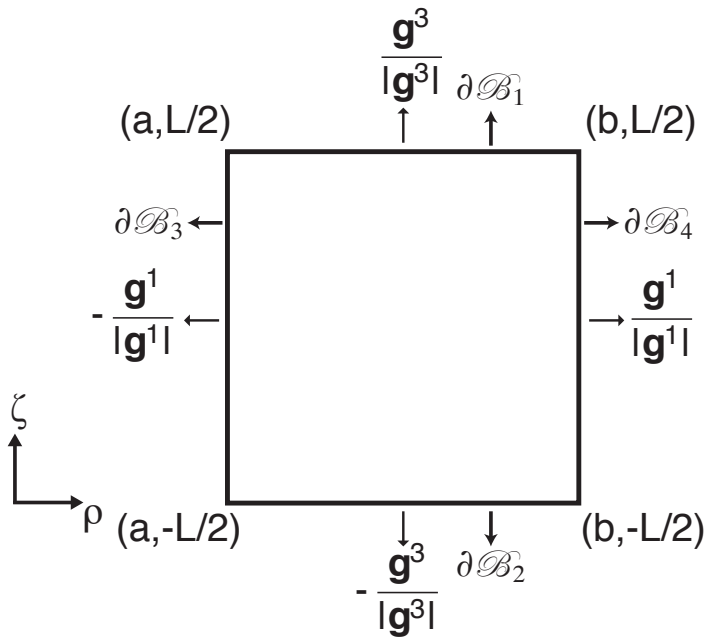

Figure 4: This schematic shows the geometry being modeled in (ρ, ζ). The contravariant vectors $-\mathbf{g}^1/|\mathbf{g}^1|$ and $\mathbf{g}^1|\mathbf{g}^1|$ are the normal vectors to the boundaries $\rho = a$ and $\rho = b$, respectively. Similarly, $-\mathbf{g}^3/|\mathbf{g}^3|$ and $\mathbf{g}^3/|\mathbf{g}^3|$ are normal vectors to the boundaries $\zeta = 0$ and $\zeta = L/2$, respectively. {fig_norm

$\tau^{ij} = \tau^{ij}(\rho, \zeta)$, so that $\partial\tau^{ij}/\partial\phi = 0$. On simplifying the equilibrium equations using the definition of the Christoffel symbols of the second kind given in eq. (29) we get, {equilibr

$$\frac{\tau^{11}}{\rho} - \rho\,\tau^{22} + \frac{\partial\tau^{13}}{\partial\zeta} + \frac{\partial\tau^{11}}{\partial\rho} = 0, \tag{54a}$$

$$3\,\frac{\tau^{12}}{\rho} + \frac{\partial\tau^{23}}{\partial\zeta} + \frac{\partial\tau^{12}}{\partial\rho} = 0, \tag{54b}$$

$$\tau^{13} - 2\,\bar{L}\,\tau^{12} + \rho\left(\frac{\partial\tau^{33}}{\partial\zeta} + \frac{\partial\tau^{13}}{\partial\rho}\right) = 0. \tag{54c}$$

We need to note that Christoffel symbols are function of ρ only. We will proceed in the next section to solve the equilibrium equations numerically using finite element method.

4. Variational formulation and finite element method in helical coordinates

In the previous sections, we have detailed the linear thermo-elastic formulation in helical coordinates. The strong form or the equilibrium equations in the absence of body force are

rong_form} given as,

$$\frac{\partial \tau^{ij}}{\partial \theta^j} + \Gamma^i_{mj}\,\tau^{mj} + \Gamma^j_{mj}\,\tau^{im} = 0, \text{ in } \mathscr{B}, \tag{55a}$$

$$u^2 = u^3 = 0, \text{ on } \partial\mathscr{B}_2, \tag{55b}$$

$$t_i = 0, \text{ on } \partial\mathscr{B}_1 \cup \partial\mathscr{B}_3 \cup \partial\mathscr{B}_4, \tag{55c}$$

$$t_1 = 0, \text{ on } \partial\mathscr{B}_2. \tag{55d}$$

It is important to note here that symmetry conditions are imposed on u^2 and u^3 at $\zeta = 0$, so that only half the geometry needs to be modeled. Therefore, the boundary $\partial\mathscr{B}_2$ can be considered to be at $\zeta = 0$ instead of $\zeta = -L/2$. We propose to solve the strong form using finite element method (FEM) invoking the variational or weak form of the equilibrium equations as given in Hughes [23]. Let u^i be the trial solution such that $u^i \in \mathcal{S}_i$, where $\mathcal{S}_i$ for $i = 1, 2, 3$ is the collection of trial solutions given by,

$$\mathcal{S}_i = \{u^i \;\big|\; u^i \in \mathrm{H}^1(\mathscr{B}),\; u^2(\rho, 0), u^3(\rho, 0) = 0\}. \tag{56}$$ {trial_sol

The symbol $\mathrm{H}^1(\cdot)$ is the Hilbert space (see [24, 23] for more details). We also define the collection of all admissible variations or test functions denoted by $\mathcal{V}_i$, which is give as,

$$\mathcal{V}_i = \{w^i \;\big|\; w^i \in \mathrm{H}^1(\mathscr{B}),\; w^2(\rho, 0), w^3(\rho, 0) = 0\}. \tag{57}$$ {test_sol

The weak formulation can be given as follows, let $\mathcal{S} = \{\mathbf{u} \mid u^i \in \mathcal{S}_i\}$, $\mathcal{V} = \{\mathbf{w} \mid w^i \in \mathcal{V}_i\}$ and given $\boldsymbol{\ell}$, find $\mathbf{u} \in \mathcal{S}$ such that for all $\mathbf{w} \in \mathcal{V}$

$$a(\mathbf{w}, \mathbf{u}) = (\mathbf{w}, \boldsymbol{\ell}), \tag{58}$$ {weak_form

where $a(\cdot, \cdot)$ and $(\cdot, \cdot)$ is symmetric, bilinear forms (see [23] for details). The symbol $\boldsymbol{\ell}$ is like a body force term. The explicit forms of $a(\mathbf{w}, \mathbf{u})$ and $(\mathbf{w}, \boldsymbol{\ell})$ are given as, {bilinear_

$$a(\mathbf{w}, \mathbf{u}) = \int_{\mathscr{B}} \frac{1}{4}\, \mathsf{C}^{ijkl} \left((u_k|_l + u_l|_k)\; \left(w_i|_j + w_j|_i\right)\right) dV, \tag{59a}$$

$$(\mathbf{w}, \boldsymbol{\ell}) = \int_{\mathscr{B}} \frac{1}{2}\, \mathsf{C}^{ijkl}\, \alpha\, \Delta T\, g_{kl} \left(w_i|_j + w_j|_i\right) dV, \tag{59b}$$

where dV is volume element in helical coordinates given by eq. (23).

4.1. Finite element formulation

We solve for the minimizer and the minima from the weak form given in bilinear and linear forms from eq. (59) using FEM. Consider $\mathcal{S}^h$ and $\mathcal{V}^h$ be the finite dimensional approximations of $\mathcal{S}$ and $\mathcal{V}$, respectively. Let $\mathbf{w}^h \in \mathcal{V}^h$ such that $(w^h)^2,\; (w^h)^3 = 0$ on $\partial\mathscr{B}_2$, so that the boundary conditions on $\mathbf{u}$ are satisfied. Assuming that the members of $\mathcal{S}^h$ admit an additive decomposition,

$$\mathbf{u}^h = \mathbf{v}^h + \mathbf{g}^h,$$

where $\mathbf{v}^h \in \mathcal{V}^h$ and $\mathbf{g}^h$ approximately satisfies $u^2 = u^3 = 0$ on $\partial\mathscr{B}_2$. Therefore, the Galerkin formulation in finite dimensional space can be expressed as, find $\mathbf{u}^h = \mathbf{v}^h + \mathbf{g}^h \in \mathcal{S}^h$ such that for all $\mathbf{w}^h \in \mathcal{V}^h$, we have

$$a\left(\mathbf{w}^h, \mathbf{v}^h\right) = \left(\mathbf{w}^h, \boldsymbol{\ell}\right). \tag{60}$$ {galerkin}

Before, we descretize the domain, we define the nomenclature that will be used in the rest of the discussion as follows,

- n_{dof} is the number of degrees of freedom per node,
- n_{np} is the total number of nodes,
- η is the set of all nodes,
- η_g is the set of nodes on the boundary where $(u^h)^i$ is prescribed,
- n_{el} is the total number of elements in the domain,
- n_{en} is the total number of nodes in an element.

Let us discretize the domain using global basis functions denoted by N_A that satisfy partition of unity, i.e., $\sum_{A=1}^{n_{\text{np}}} N_A = 1$ (see [23]). Further, N_A are spatial functions of (ρ, ζ). The nodal coefficients to be determined are denoted as d_{iA} and the arbitrary constants as c_{iA}. The trial and test functions can be expressed as, {vw_comp}

$$\left(v^h\right)^i = \sum_{A \in \eta - \eta_g}^{n_{\text{np}}} N_A \; d_{iA}, \tag{61a}$$

$$\left(g^h\right)^i = \sum_{A \in \eta_g}^{n_{\text{np}}} N_A \; g_{iA}, \tag{61b}$$

$$\left(w^h\right)^i = \sum_{A \in \eta - \eta_g}^{n_{\text{np}}} N_A \; c_{iA}. \tag{61c}$$

The vector version of the above equations in the helical basis is, finite_vw}

$$\mathbf{v}^h = \left(v^h\right)^i \; \mathbf{g}_i, \tag{62a}$$

$$\mathbf{g}^h = \left(g^h\right)^i \; \mathbf{g}_i, \tag{62b}$$

$$\mathbf{w}^h = \left(w^h\right)^i \; \mathbf{g}_i. \tag{62c}$$

We can substitute the above equations into the Galerkin form given in eq. (60) and simplify it using bilinearity properties we get,

$$\sum_{j=1}^{n_{\text{dof}}} \left(\sum_{B \,\in\, \eta - \eta_g} a\left(N_A \; \mathbf{g}_i, N_B \; \mathbf{g}_j\right) \; d_{jB} \right) = \left(N_A \; \mathbf{g}_i, \; \boldsymbol{\ell}\right), \tag{63}$$ galerkin}

where $A \in \eta - \eta_g$ and $1 \leq i \leq 3$. This above equation can be expressed in matrix form as,

$$\mathbf{Kd} = \mathbf{F},$$

where $\mathbf{K} = [K_{PQ}]$ is the global stiffness matrix, $\mathbf{d} = \{d_Q\}$ is the nodal displacement vector and $\mathbf{F} = \{F_P\}$ is global force vector. The global stiffness matrix and force vector in component forms are,

$$K_{PQ} = a\left(N_P\, \mathbf{g}_i, N_Q\, \mathbf{g}_j\right),$$
$$F_P = \left(N_P\, \mathbf{g}_i, \boldsymbol{\ell}\right).$$

4.2. Local description FEA

The Galerkin form given in eq. (63) is in global description i.e., the shape functions N_A are spatial functions of (ρ, ζ). However, a serious drawback of using these shape functions is that they would have to be derived every time the number of elements are modified (see [25] for additional details on the disadvantages). It is more straight forward to solve the set of equations using local description of shape functions i.e., N_a which are functions of local coordinate system $(\xi_1,\ \xi_2)$ (see [23, 25]). The global domain and local domain are related by an affine transformation $T : [\rho, \zeta] \rightarrow [\xi_1,\ \xi_2]$ such that $T(\rho, \zeta) = (\xi_1,\ \xi_2)$. The global domain is illustrated by Fig. 5(a), where the red circles denote the global node number A and the shape functions N_A are global shape functions which are spatial functions of (ρ, ζ). In order to do calculations in the local coordinates system, the domain is divided into elements $e = \{1, n_{\text{el}}\}$ given by the solid black lines. Once such element occupying a volume Ω^e is highlighted using the dashed grey box as shown in the figure. 5(a). A magnified version of the element is shown in Fig. 5(b), in the local coordinates system $(\xi_1,\ \xi_2)$, where $\{(\xi_1,\ \xi_2) : \xi_1,\ \xi_2 \in [-1, 1]\}$. The element has 8 nodes, 4 corner (solid black circles) and 4 mid-side (black hollow circles) and the coordinates at a node a are denoted as $(\xi_1^a,\ \xi_2^a)$. The local node numbers a are given in magenta color. The element is commonly called the 8 noded serendipity element (see [25] for details). The local shapes functions are denoted by N_a, where $a = \{1, n_{\text{en}}\}$ and in this case $n_{\text{en}} = 8$. The general expression for the shape functions for the eight-noded element are taken from [25] and at the corner nodes, i.e., $a = \{1, 2, 3, 4\}$, are,

$$N_a\left(\xi_1, \xi_2\right) = \frac{1}{4}\left(1 + \xi_1^a\, \xi_1\right)\left(1 + \xi_2^a\, \xi_2\right)\left(-1 + \xi_1^a\, \xi_1 + \xi_2^a\, \xi_2\right), \tag{64}$$

where $\xi_1^a,\ \xi_2^a$ can be obtained from the Fig. 5, specifically to be $\{\xi_1^1,\ \xi_1^2,\ \xi_1^3,\ \xi_1^4\} = \{-1, 1, 1, -1\}$ and $\{\xi_2^1,\ \xi_2^2,\ \xi_2^3,\ \xi_2^4\} = \{-1, -1, 1, 1\}$, respectively. The general expression for the shape functions at mid-side nodes, i.e., $a = \{5, 6, 7, 8\}$,
if $\xi_1^a = 0$,

$$N_a\left(\xi_1, \xi_2\right) = \frac{1}{2}\left(1 - (\xi_1)^2\right)\left(1 + \xi_2^a\, \xi_2\right)), \tag{65}$$

if $\xi_2^a = 0$,

$$N_a\left(\xi_1, \xi_2\right) = \frac{1}{2}\left(1 + \xi_1^a\, \xi_1\right)\left(1 - (\xi_2)^2\right). \tag{66}$$

Further, for the local basis (ξ_1, ξ_2) we adopt the convention given in [23] and replace subscripts $A, B, ...$ with $a, b, ...$, and a superscript e is introduced to make it clear that element level computations are being performed. The global stiffness matrix and global force vector can be expressed as summations from the elemental counterparts as follows,

$$
\begin{aligned}
[K_{AB}] &= \sum_{e=1}^{n_{\text{el}}} [k^e_{ab}], \\
\{F_A\} &= \sum_{e=1}^{n_{\text{el}}} \{f^e_a\},
\end{aligned}
\tag{67}
$$

where k^e_{ab} and f^e_a are the elemental stiffness matrix and force vector, respectively and are defined as follows,

$$
\begin{aligned}
k^e_{ab} &= a\,(N_a, N_b)^e\,, \\
f^e_a &= (\ell, N_a)^e\,.
\end{aligned}
\tag{68}
$$

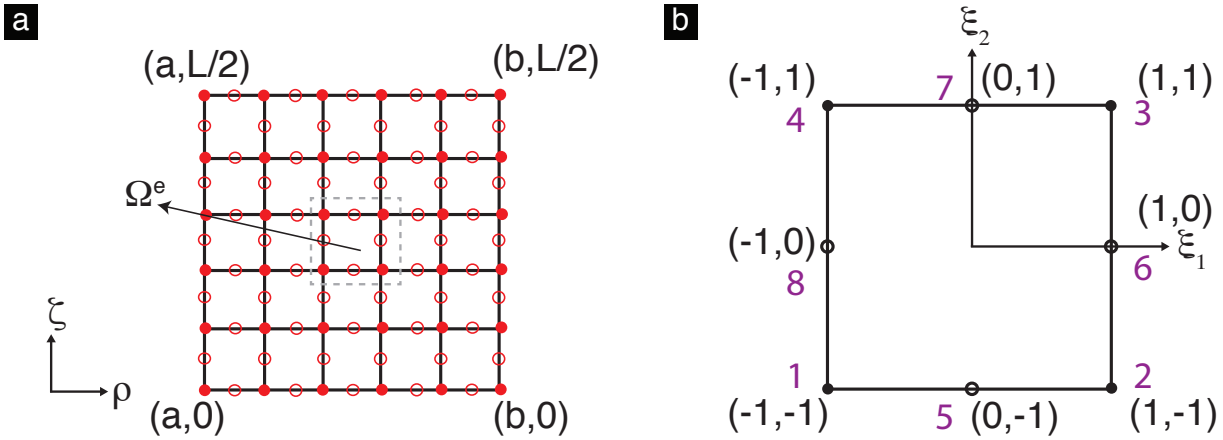

Figure 5: The domain with the global coordinate system (ρ, ζ) is shown in subfigure (a). Further, only half the domain is shown i.e., $(\rho, \zeta) : \rho \in [a, b], \zeta \in [0, L/2])$. The domain as can be seen is made of elements where the red circles are the global nodes. Subfigure (b) shows the dashed region from subfigure (a), with an element in its local coordinate system (ξ_1, ξ_2), where the dark black circles are local corner nodes and the hollow circles are mid-side nodes.

{fig:1}

5. Results and discussion

In this section, we solve the boundary value problem numerically, specifically by choosing the temperature distribution $\Delta T = \Delta T_0\, \rho$, where ΔT_0 is a scaling constant. We compute the the non-dimensionlized strain energy $\Pi / E(\alpha \Delta T_0)^2 V$ by varying $\bar{L}/a$ and b/a. Further, we also investigate the dependence of the strain energy on the Poissons ratio of the material. We also derive an approximate analytical solution which is an upper bound to the non-dimensionalized

strain energy using the Ritz's method. We make an educated guess for the displacement field such that the boundary conditions are satisfied and solve for the coefficients of the the guess functions by minimizing the strain energy.

5.1. Numerical solution

The boundary value problem described in section using finite element method described in section 3. Symmetry conditions are imposed on the displacement components $u^2, u^3 = 0$ on the boundary $\partial\mathscr{B}_2$ (i.e., $\zeta = 0$) and an illustration of the boundary value problem (bvp) is shown in Fig. 6(a). The scaling constant $\Delta T_0 = 1$ and the coefficient of thermal expansion $\alpha = 1$ in all computations. The computations are performed for $b/a = \{2, 3, 4, 5\}$ and $L/a = (0.02, 200)$. Representative contour plots of the displacement field u^1, u^2, u^3 is shown in Fig. 6 (b), (c), (d), respectively for the case of $a = 0.5$, $b = 1.0$ and $L = 1.0$. Similarly, the contravariant components of the Cauchy stress tensor τ^{ij} is shown in Fig. 7 .

5.1.1. Verification of the numerical solution

5.1.2. Traction boundary conditions

We compute the traction on the boundaries of the domain $\partial\mathscr{B}$ to check if the traction is zero on the boundaries where neither traction nor displacement is prescribed. The traction vector on the boundaries is given in eq. (53). Displacement boundary conditions $u^2 = u^3 = 0$ are imposed on the boundary $\partial\mathscr{B}_2$, therefore, the obtained solution to displacement fields from the finite element computation should satisfy, {traction_

$$\tau_1^{\cdot 3} = \tau_2^{\cdot 3} = \tau_3^{\cdot 3} = 0 \text{ at } \zeta = L/2, \tag{69a}$$

$$\tau_1^{\cdot 1} = \tau_2^{\cdot 1} = \tau_3^{\cdot 1} = 0 \text{ at } \rho = a, b, \tag{69b}$$

$$\tau_1^{\cdot 3} = 0 \text{ at } \zeta = 0. \tag{69c}$$

We can verify whether the traction vector obtained from the FEA solution satisfies traction free boundary condition. Let us consider the boundaries $\rho = a, b$, and for the boundaries to be traction free, Cauchy stress components $\tau_1^{\cdot 1}$, $\tau_2^{\cdot 1}$ and $\tau_3^{\cdot 1}$ have to be zero as given eq. (69). On plotting these components along $\rho \in [a, b]$, where $a = 0.5$ and $b = 1.0$ as shown in Fig. 8(a), (b) and (c). In each subfigure, each of the traction vectors is plotted at $\zeta = 0.1, 0.25, 0.41$ in red, blue and black solid lines, respectively. It is evident that the traction vector components are almost zero at the boundaries $\rho = a$ and $\rho = b$, respectively. Similarly, we consider the traction vector components on $\zeta = 0$ and $\zeta = L/2$ boundaries. From the Fig. 8(d), (e) and (f), it can be seen that Cauchy stress component $\tau_1^{\cdot 3}$ is almost zero at $\zeta = 0, L/2$. Further, components $\tau_2^{\cdot 3}$ and $\tau_3^{\cdot 3}$ are almost zero at $\zeta = L/2$ which is consistent with what is given in eq. (69).

5.1.3. Nodal forces

In the section, to verify whether equilibrium is indeed satisfied, we compute the nodal forces to verify that they are indeed almost zero everywhere. Let us consider the strong form

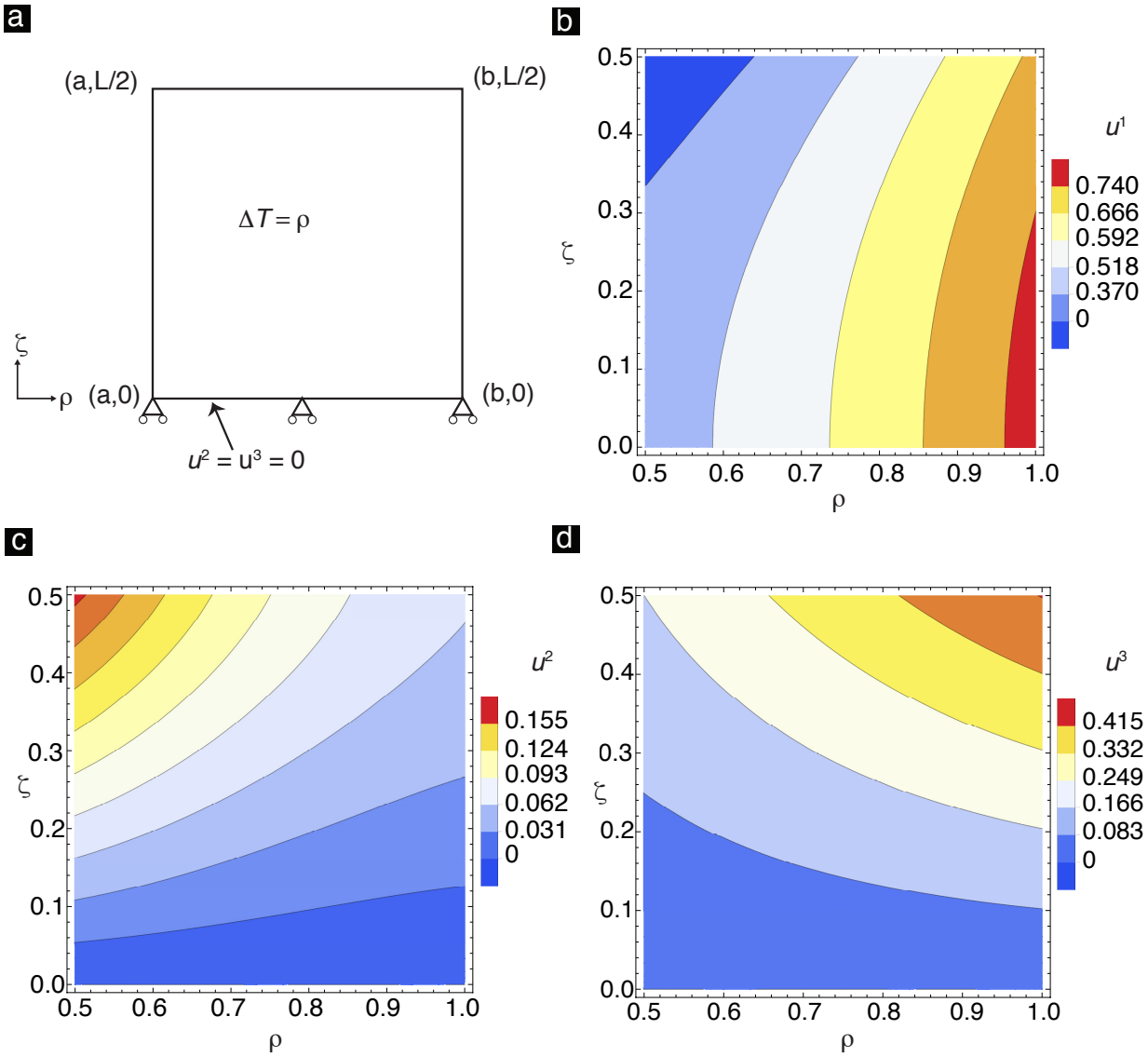

Figure 6: In this figure, a schematic of the boundary value problem is shown in subfigure (a), where $u^2 = u^3 = 0$ at $\zeta = 0$ and $\Delta T = \rho$ is the prescribed temperature distribution. The contour plots for the case of $a = 0.5$, $b = 1.0$ and $L = 1.0$ for the computed displacement components u^1, u^2 and u^3 are presented in the subfigures (b), (c) and (d), respectively. {fig_disp

eq. 55, where the equilibrium equations are expressed using the mixed form of Cauchy stress tensor $\tau_i^{\cdot j}$. The divergence of $\boldsymbol{\tau}$ in helical coordinates is given as,

$$\text{div}\,\boldsymbol{\tau} = \tau_i^{\cdot j}\,\big|_j\;\mathbf{g}^i,$$

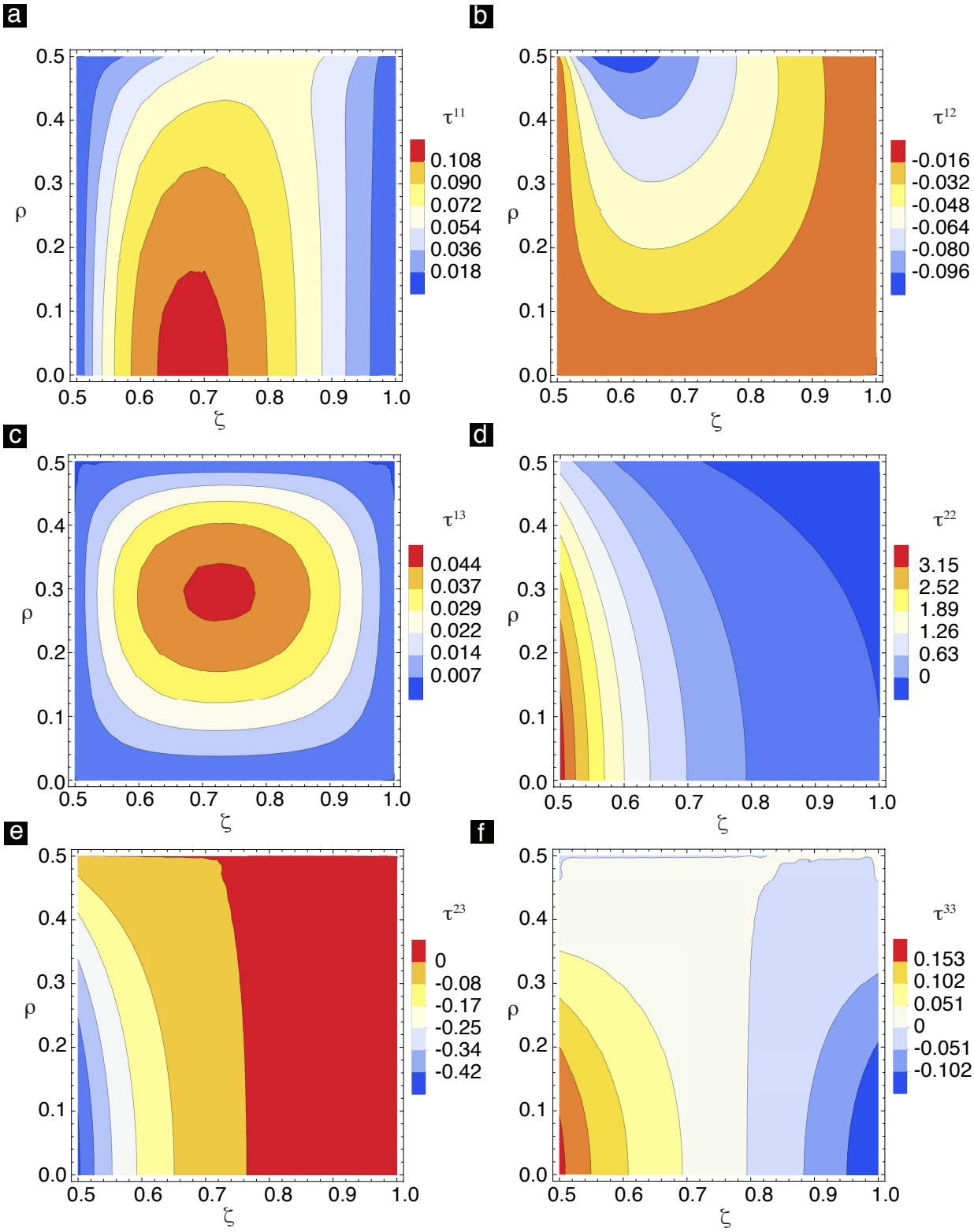

Figure 7: In this figure the contour plots for the Cauchy stress components τ^{11}, τ^{12}, τ^{13}, τ^{22}, τ^{23} and τ^{33} are presented in the subfigures (a), (b), (c), (d), (e) and (f), respectively. {fig_stres

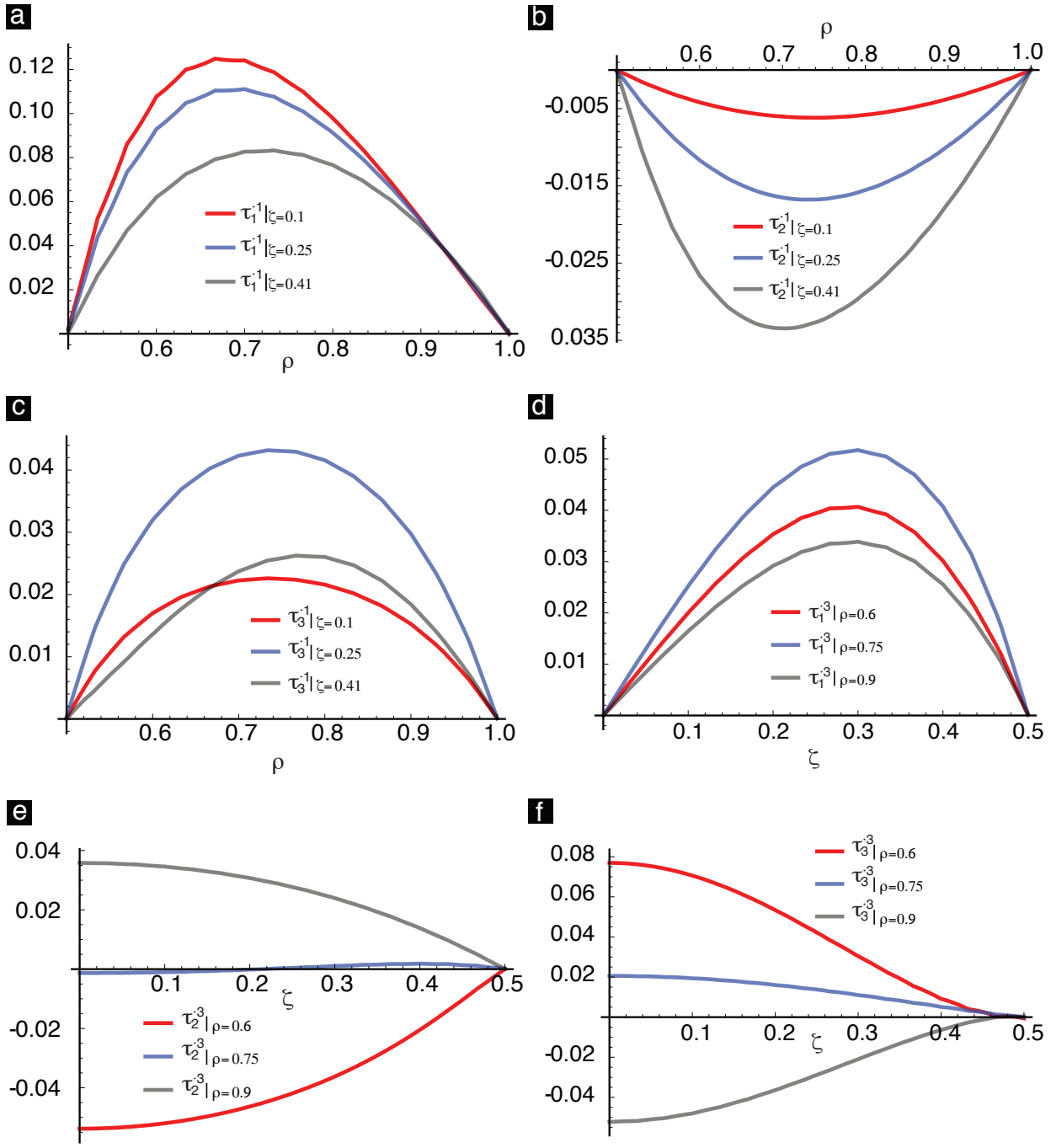

Figure 8: In subfigure (a), (b) and (c) Cauchy stress components $\tau^1_{\cdot 1}$, $\tau^2_{\cdot 1}$, $\tau^3_{\cdot 1}$ are plotted along $\rho \in [a, b]$, where a = 0.5 and b = 1.0, respectively. Further, the components are plotted at $\zeta = 0.1, 0.25$ and 0.41, denoted by red, blue and black solid lines, respectively. Similarly, subfigure (d), (e) and (f) Cauchy stress components $\tau^1_{\cdot 3}$, $\tau^2_{\cdot 3}$, $\tau^3_{\cdot 3}$ are plotted along $\zeta \in [0, L/2]$, where L = 1.0, respectively. Further, the components are plotted at $\rho = 0.6, 0.75$ and 0.9, denoted by red, blue and black solid lines, respectively {fig_trac

where,

$$\tau_i^{\cdot j}\,\big|_j = \left(\frac{\partial \tau_i^{\cdot j}}{\partial \theta^j} + \Gamma^j_{mj}\,\tau_i^{\cdot m} - \Gamma^m_{ij}\,\tau_m^{\cdot j}\right).$$

Consider a test function $w^i \in \mathcal{V}_i$ as before, we get the weak form to be,

$$R = \int_{\mathscr{B}} \tau_i^{\cdot j}\,\big|_j\; w^i\, dV,$$
$$R = \int_{\mathscr{B}} \left(\frac{\partial \tau_i^{\cdot j}}{\partial \theta^j} + \Gamma^j_{mj}\,\tau_i^{\cdot m} - \Gamma^m_{ij}\,\tau_m^{\cdot j}\right) w^i\,\rho\, d\rho\, d\phi\, d\zeta,$$

on using the divergence theorem (see [19] for more details), we get

$$R = -\int_{\mathscr{B}} \tau_i^{\cdot j}\,\frac{\partial\left(w^i\,\rho\right)}{\partial \theta^j}\, d\rho\, d\phi\, d\zeta + \int_{\partial\mathscr{B}} t_i\, w^i\, dS + \int_{\mathscr{B}} \left(\Gamma^j_{mj}\,\tau_i^{\cdot m} - \Gamma^m_{ij}\,\tau_m^{\cdot j}\right) w^i\,\rho\, d\rho\, d\phi\, d\zeta,$$

where t_i are the components of the traction vector on the boundary $\partial\mathscr{B}$ and dS is the area element. The test function can be expressed using shape functions N^A and arbitrary coefficients c_{iA} as before in eq. (61) and the stress components $\tau_i^{\cdot j}$ and the traction components t_i can computed using the displacement field obtained from the numerical solution, i.e., $\mathbf{u}^h$ and then the nodal forces R_i for $i = 1, 2, 3$ can be expressed as,

$$R_i = -\int_{\mathscr{B}} \tau_i^{\cdot j}\left(\left(u^i\right)^h\right)\,\frac{\partial\left(N^A\,\rho\right)}{\partial \theta^j}\, d\rho\, d\phi\, d\zeta + \int_{\partial\mathscr{B}} t_i\left(\left(u^i\right)^h\right)\, N^A\, dS + \int_{\mathscr{B}} \left(\Gamma^j_{mj}\,\tau_i^{\cdot m} - \Gamma^m_{ij}\,\tau_m^{\cdot j}\right)\, N^A\,\rho\, d\rho\, d\phi\, d\zeta, \tag{70}$$

{nodal_ve

For equilibrium to hold the nodal forces R_i has to be almost zero at every node in the domain. The nodal force vector is computed and assembled using the local FEA description given in section 3. The components R_1, R_2 and R_3 are plotted over the domain $\mathscr{B}$ in Fig. 9 and it can be seen that the nodal forces are of the order $1e-5$. Thus, we can conclude that the solution is accurate and satisfies equilibrium within a numerical tolerance of $1e-5$.

5.2. Elastic strain energy variation

We compute elastic strain energy Π given by eq. (48b) from numerically obtained displacement fields. The non-dimensionlized form of elastic strain energy $\Pi/E(\alpha\Delta T_0)^2V$ per unit volume V is plotted against $\bar{L}/a$ as shown in figure. The energy curve for various b/a approach a limit, respectively for large $\bar{L}/a$ and the limit is higher as the ratio of b/a increases. Further, as $\bar{L}/a$ is small, the energy approaches 0. Therefore, we have asymptotic limits for $\bar{L}/a \to 0$ and $\bar{L}/a \to \infty$. We also study the dependence of Poisson's ratio on energy curve as shown in the figure for $b/a = 2$ and $\nu = \{0.1, 0.25, 0.4\}$. It can be seen that that there is almost no appreciable difference in the different curves. Further, the asymptotic limits for the all the curves are identical.

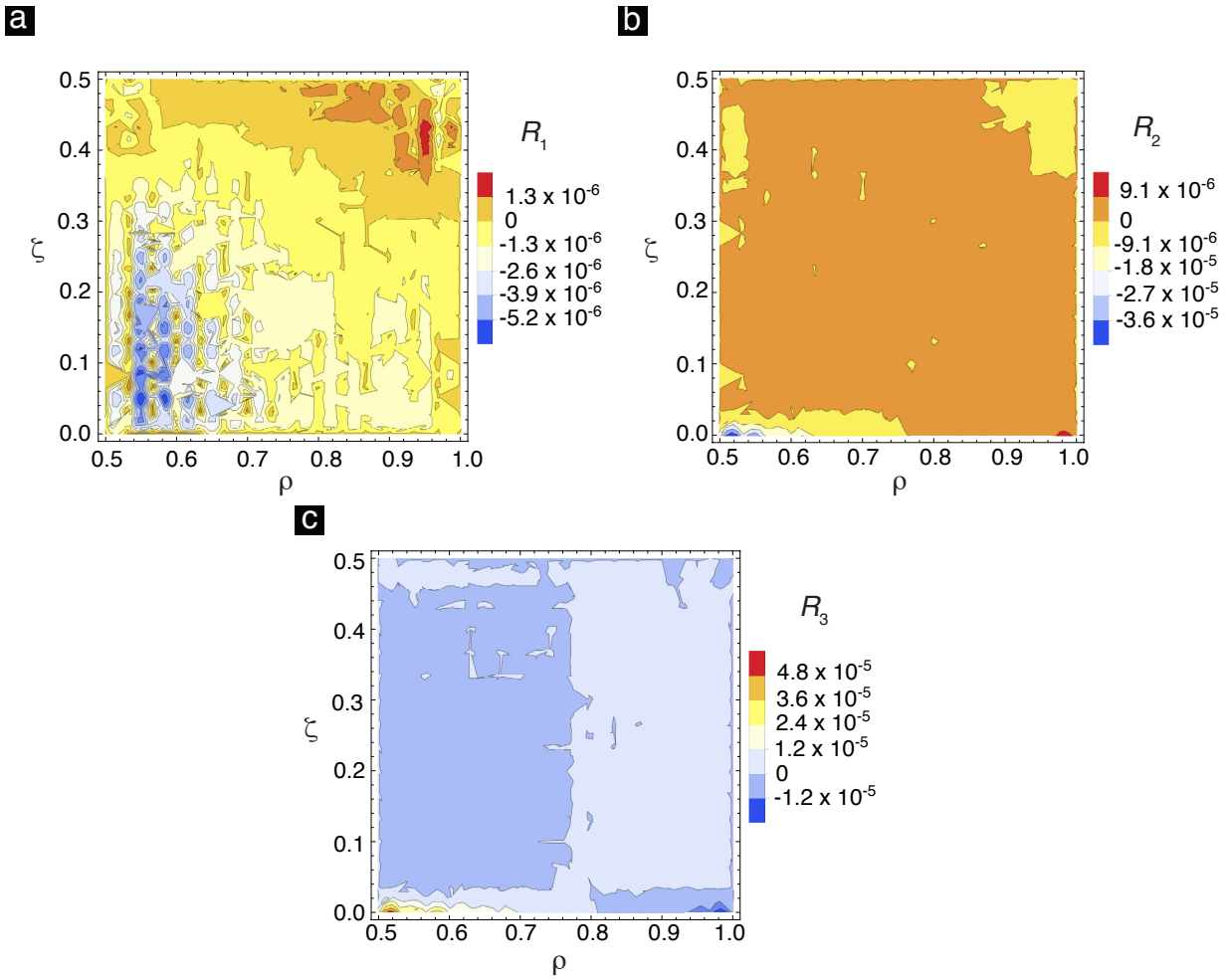

Figure 9: In this figure the nodal forces are computed as given in eq. (70) using FEA and plotted over domain $\rho \in [0.5, 1]$ and $\zeta \in [0, 0.5]$. The nodal force components R_1, R_2 and R_3 are plotted in subfigures (a), (b) and (c), respectively. {fig:noda

5.3. Analytical solution

In this section, we propose an analytical solution for the energy curve shown in Figure . To derive the analytical solution we propose to employ Ritz's method. We guess the displacement field as follows:

$$u_g^1 = C_1 + C_2\,\rho^2, \tag{71}$$

$$u_g^2 = C_3\,\zeta + C_4\,\rho\,\zeta, \tag{72}$$

$$u_g^3 = C_5\,\zeta, \tag{73}$$

where, C_1, C_2, C_3, C_4, C_5 are arbitrary constants which need to be solved for by minimizing the energy computed from these fields. It is important to note that the above mentioned displacement fields satisfy the bcs i.e., u_g^2, $u_g^3 = 0$ at $\zeta = 0$. The energy computed from the the

guess displacement field should form an enevelope over the numerical solution because the guess displacement field are not the actual minimizers to the BVP, therefore, the computed energy should be greater than the FEA solution. We employ the eq. (48b) to compute the energy over the domain $\Omega = \{(\rho, \zeta) \ : \ \rho \in [a, b], \ \zeta \in (-L/2, L/2)\}$. Let the computed energy be denoted by Π_g, we solve for the constants C_1, C_2, C_3, C_4, C_5 by setting $\partial \Pi_g / \partial C_i = 0$ for $i = 1, 2, 3, 4, 5$ solving for the constants simultaneously. Once we do that we get C_i to be. We can plot the analytical solution for $b/a = 2$ and compare against the numerical solution for energy as shown in Figure . It can be clearly seen that the analytical solution (given by the solid line) is approximately close to the numerical data and is an upper bound the numerical solution obtained from FEA as we had expected.

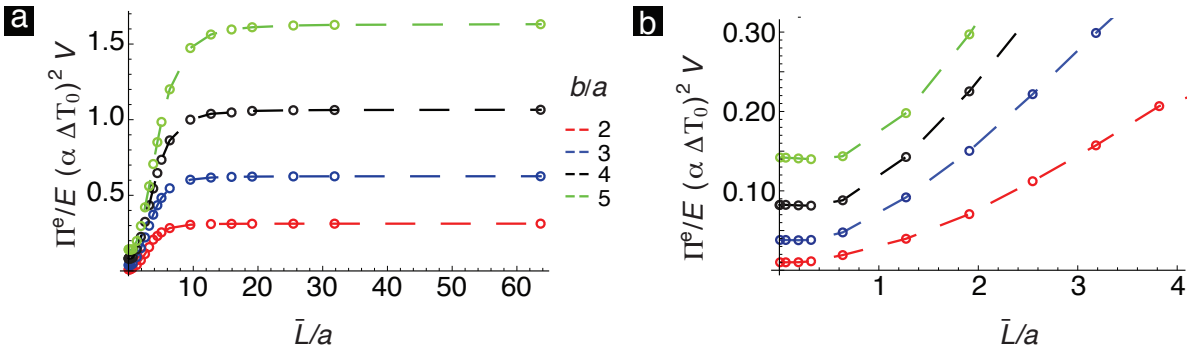

Figure 10: The variation of non-dimensionalized energy $\Pi^e/E(\alpha\Delta T_0)^2 V$ with $\bar{L}/a$ for various ratios of b/a is shown. The subfigure (b), is an enlarged view of the energy curves for small $\bar{L}/a$. {fig:2}

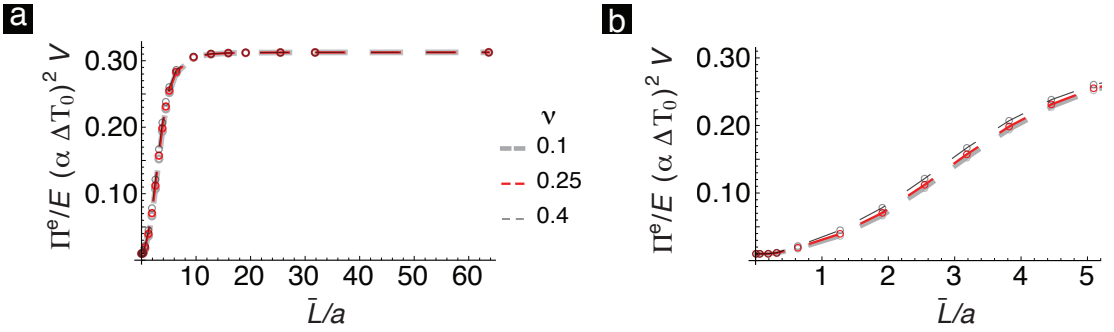

Figure 11: The variation of non-dimensionalized energy $\Pi^e/E(\alpha\Delta T_0)^2 V$ with $\bar{L}/a$ for Poisson's ratio $\nu = \{0.1, 0.25, 0.4\}$ is shown. The subfigure (b), is an enlarged view of the energy curves for small $\bar{L}/a$. {fig:3}

References

[1] D. Hull, Fractography: observing, measuring and interpreting fracture surface topography, Cambridge University Press, 1999.

[2] L. Goehring, Evolving fracture patterns: columnar joints, mud cracks and polygonal terrain, Phil. Trans. R. Soc. A 371 (2004) (2013) 20120353.

[3] P. Plummer, V. Gostin, Shrinkage cracks: desiccation or synaeresis?, Journal of Sedimentary Research 51 (4).
[4] R. D. Deegan, S. Chheda, L. Patel, M. Marder, H. L. Swinney, J. Kim, A. de Lozanne, Wavy and rough cracks in silicon, Physical Review E 67 (6) (2003) 066209.
[5] R. D. Deegan, P. J. Petersan, M. Marder, H. L. Swinney, Oscillating fracture paths in rubber, Physical review letters 88 (1) (2001) 014304.
[6] M. HIRATA, Experimental studies on form and growth of cracks in glass plate, Scientific Papers of Institute of Physical and Chemical Research 16 (1931) 172–195.
[7] K. Fujimoto, T. Shioya, On the wavy crack propagation behavior in internally pressurized brittle tube, JSME International Journal Series A Solid Mechanics and Material Engineering 48 (4) (2005) 178–182.
[8] Z. Neda, L. Jozsa, M. Ravasz, et al., Spiral cracks in drying precipitates, Physical review letters 88 (9) (2002) 095502.
[9] K.-T. Leung, L. Jozsa, M. Ravasz, Z. Neda, Pattern formation: Spiral cracks without twisting, Nature 410 (6825) (2001) 166.
[10] M. Sendova, K. Willis, Spiral and curved periodic crack patterns in sol-gel films, Applied Physics A 76 (6) (2003) 957–959.
[11] J. J. Hopfield, Spiral cracks in glass tubes, Nature 158 (4017) (1946) 582.
[12] J. Gillham, P. Reitz, Spiral and helical fractures, Polymer Engineering & Science 8 (3) (1968) 227–234.
[13] I. Zlotnikov, D. Shilo, Y. Dauphin, H. Blumtritt, P. Werner, E. Zolotoyabko, P. Fratzl, In situ elastic modulus measurements of ultrathin protein-rich organic layers in biosilica: towards deeper understanding of superior resistance to fracture of biocomposites, RSC Advances 3 (17) (2013) 5798–5802.
[14] J. C. Weaver, G. W. Milliron, P. Allen, A. Miserez, A. Rawal, J. Garay, P. J. Thurner, J. Seto, B. Mayzel, L. J. Friesen, et al., Unifying design strategies in demosponge and hexactinellid skeletal systems, The Journal of Adhesion 86 (1) (2010) 72–95.
[15] L. Freund, K. Kim, Spiral cracking around a strained cylindrical inclusion in a brittle material and implications for vias in integrated circuits, MRS Online Proceedings Library Archive 226.
[16] Z. C. Xia, J. W. Hutchinson, Crack patterns in thin films, Journal of the Mechanics and Physics of Solids 48 (6-7) (2000) 1107–1131.
[17] A. Argon, Surface cracks on glass, in: Proc. R. Soc. Lond. A, Vol. 250, The Royal Society, 1959, pp. 472–481.
[18] D. A. Dillard, J. A. Hinkley, W. S. Johnson, T. L. S. Clair, Spiral tunneling cracks induced by environmental stress cracking in larcâĎć-tpi adhesives, The Journal of Adhesion 44 (1-2) (1994) 51–67.
[19] M. E. Gurtin, An introduction to continuum mechanics, Vol. 158, Academic press, 1982.
[20] C. S. Jog, Continuum mechanics, Vol. 1, Cambridge University Press, 2015.
[21] A. E. Green, W. Zerna, Theoretical elasticity, Courier Corporation, 1992.
[22] P. Overfelt, Helical harmonics for static fields, Physical Review E 64 (3) (2001) 036603.
[23] T. J. Hughes, The finite element method: linear static and dynamic finite element analysis, Courier Corporation, 2012.
[24] L. C. Evans, Weak convergence methods for nonlinear partial differential equations, no. 74, American Mathematical Soc., 1990.
[25] O. C. Zienkiewicz, R. L. Taylor, O. C. Zienkiewicz, R. L. Taylor, The finite element method, Vol. 3, McGraw-hill London, 1977.